

# Author Manuscript

This is the author manuscript accepted for publication and has undergone full peer review but has not been through the copyediting, typesetting, pagination and proofreading process, which may lead to differences between this version and the [Version of Record](#). Please cite this article as [doi: 10.1111/joa.12632](https://doi.org/10.1111/joa.12632)

This article is protected by copyright. All rights reserved

# The effect of age and demographics on rib shape

Sven A. Holcombe,<sup>\*,†,‡</sup> Stewart C. Wang,<sup>‡</sup> and James B. Grotberg<sup>†</sup>

<sup>†</sup>*Department of Biomechanical Engineering, University of Michigan, Ann Arbor, MI, USA*

<sup>‡</sup>*International Center for Automotive Medicine, University of Michigan, Ann Arbor, MI, USA*

E-mail: [svenho@umich.edu](mailto:svenho@umich.edu)

Author Manuscript

## Abstract

Elderly populations have higher risk of rib fractures and other associated thoracic injuries than younger adults, and the changes in body morphology that occur with age are a potential cause for this increased risk.

Rib centroidal path geometry for 20,627 ribs was extracted from computed tomography (CT) scans of 1042 live adult subjects, then fit to a six-parameter mathematical model that accurately characterizes rib size and shape, and a three-parameter model of rib orientation within the body. Multivariable regression characterized the independent effect of age, height, weight, and sex on the rib shape and orientation across the adult population, and statistically significant effects were seen from all demographic factors ( $p < 0.0001$ ).

This study reports a novel aging effect whereby both the rib end-to-end separation and rib aspect ratio are seen to increase with age, producing elongated and flatter overall rib shapes in elderly populations, with age alone explaining up to 20% of population variability in the aspect ratio of mid-level ribs. Age was not strongly associated with overall rib arc length, indicating that age effects were related to shape change rather than overall bone length. The rib shape effect was found to be more strongly and directly associated with age than previously documented age-related changes in rib angulation. Other demographic results showed height and sex being most strongly associated with rib size, and weight most strongly associated with rib pump-handle angle.

Results from the study provide a statistical model for building rib shapes typical to any given demographic by age, height, weight, and sex, and can be used to help build population-specific computational models of the thoracic rib cage. Furthermore, results also quantify normal population ranges for rib shape parameters which can be used to improve the assessment and treatment of rib skeletal deformity and disease.

## Introduction

2 Rib fractures and chest injuries are particularly problematic for elderly individuals. They experience both  
a greater likelihood of sustaining fractures than younger cohorts<sup>1</sup> and poorer clinical outcomes including  
4 longer stays in intensive care facilities resulting in a greater overall economic burden<sup>2</sup>. Overall, chest  
injuries including rib fractures most often occur due to high energy traumatic events, with motor vehicle  
6 crashes (MVCs) accounting for between 46 % to 65 % of severe injuries, and falls accounting for 21 %  
to 27 %<sup>3-5</sup>. Low energy injuries become more prevalent in the elderly, with falls accounting for 70 % of

8 geriatric trauma<sup>6</sup>. Implicating factors in chest injuries have been found, with reduced bone mineral density  
and heavy alcohol use each contributing to the risk of rib fractures<sup>7</sup>.

10 In researching such injuries, computational human body models are being increasingly used for impact  
and injury simulation of the chest and thorax. These models are largely based on the internal anatomy of  
12 selected individuals, usually chosen to represent the average external anatomy of a chosen demographic -  
most often, for example, an average-sized adult male. A recent review of computational models<sup>8</sup> identifies a  
14 current need for a more diverse modeling approach whereby at-risk or vulnerable populations are specifically  
included in modeling efforts. Elderly occupants, female occupants, obese occupants, and children are all  
16 identified as having greater risk of injury in particular body regions. In order to build such models and  
provide them the fidelity to model a diverse population, a clear understanding of the geometric variation  
18 within the population is required.

Kent et al.<sup>9</sup> first described an age effect on rib angulation in an adult male population. Ribs were  
20 found to rotate more horizontally in the sagittal plane with age, from a ninth rib angle of 50° in an 18-  
year-old to 57° in an 89-year-old. Further efforts to quantify rib and rib cage shape have followed one of  
22 two general methodologies. The first takes landmarks placed strategically across the rib cage from a series  
of individuals, then uses a combination of generalized Procrustes analysis (GPA) and principal component  
24 analysis (PCA) to quantify changes in those landmarks across populations. Gayzik et al.<sup>10</sup> used GPA to  
analyze 106 landmarks from 63 adult male rib cages<sup>10,11</sup> and described a rounding of the rib cage with  
26 aging. Weaver et al.<sup>12</sup> used a similar technique with a more complete set of landmarks across the rib cage,  
and applied it to a larger population including 164 adults and 175 children to quantify rib cage morphology  
28 changes as a whole, reporting increased rib angles and a rounding of the rib cage with age. Shi et al.<sup>13</sup> and a  
follow-up study by Wang et al.<sup>14</sup> applied GPA and PCA to landmarked rib cages from 89 and 101 subjects,  
30 respectively, and confirmed an increase in rib angle with age along with increased rib cage depth coupled  
with reduced rib cage width. While techniques such as GPA and PCA provide an overall quantification of  
32 the rib cage, their results usually combine the changes in bone shape with the changes in bone position and  
orientation, and the large number of resulting coefficients can be difficult to interpret.

34 A second general methodology isolates the ribs themselves and characterizes their shapes using mea-  
sures from geometric primitives. Examples include rib shape representations using a circular ring<sup>15</sup>, an  
36 arc<sup>16</sup>, an ellipse<sup>17</sup>, and a pair of superimposed arcs<sup>18,19</sup>. Two recent models have provided the additional  
capability of fully recreating the underlying rib shape from their parameters alone. Kindig and Kent<sup>20</sup>

38 presented a seven-parameter model with a circle and semi-ellipse connected by short patches<sup>20,21</sup>. Using  
connected spirals as the model primitives, Holcombe et al.<sup>22</sup> provided the additional benefits of simplifying  
40 the parameter space (with one fewer parameters and fewer joining patches), and using parameters that were  
themselves direct geometric properties of ribs such as their size, aspect ratio, and skewness. This meant that  
42 any rib rebuilt using statistically average parameter values from a population would itself reflect the average  
geometric properties from within that same population. To date, these direct models of rib shape have not  
44 been applied to large adult populations for the study of changes with age, however experimental studies of  
isolated ribs under loading have reported significant changes in rib stiffness and fracture onset with age<sup>23</sup>.

46 The objective of the current study is to quantify the rib shape and orientation variation present in adults,  
and to highlight the specific changes in human ribs that come as a result of aging. This was accomplished  
48 by applying the six-parameter rib shape model described in Holcombe et al.<sup>22</sup> along with measures of rib  
orientation to a large subject pool (20,627 ribs from 507 females and 535 males) that is representative of  
50 the adult population. Regression analysis of parameter trends then characterized rib morphology variation  
by demographic predictors of age, height, weight, and sex, and in particular tested the hypothesis that there  
52 is a significant aging effect on the size, shape, and orientation of ribs that occurs independently of other  
general demographics. A final outcome of this study is a parsimonious model of overall rib shape that  
54 allows researchers to build statistically representative rib geometry for any chosen subject demographic.

## Methods

### Study population

56 Under IRB HUM00041441, human rib centroidal path geometry was extracted from 507 female and 535  
58 male CT scans in the International Center for Automotive Medicine (ICAM) morphomics database. Scans  
were from adult patients (20 to 99 years of age) who entered a Level 1 trauma center between 2000 and 2016  
60 and underwent abdomen and/or chest CT scanning as part of their normal course of diagnosis and treatment.  
Scans exhibiting skeletal abnormality (including scoliosis, kyphosis, spine or rib fixation devices, bifurcat-  
62 ing ribs or abnormal rib counts) were excluded, as were fractured ribs (see below). Of the patients meeting  
scan inclusion criteria, the majority were admitted due to MVCs (78 %) and falls (7 %). The study popu-  
64 lation demographics are shown by sex in Figure 1, and compared to the CDC's anthropometric reference  
data for North American adults over 20 years of age from 2007-2010<sup>24</sup> in Table 1, with heights and weights

66 generally differing by less than 0.1 standard deviations between the current study and the CDC comparison populations.

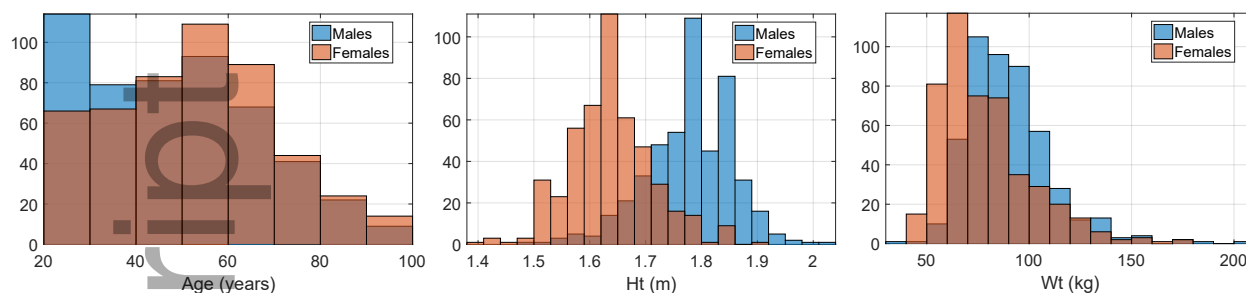


Figure 1: Population histograms showing the age, height and weight distributions for males and females within the studied population.

Table 1: Study demographics mean and percentiles (in bold), along with CDC reference population data in parentheses<sup>24</sup>.

	Mean	Std.	5 <sup>th</sup>	10 <sup>th</sup>	25 <sup>th</sup>	50 <sup>th</sup>	75 <sup>th</sup>	90 <sup>th</sup>	95 <sup>th</sup>
<b>Males (N = 535)</b>									
Weight, kg	<b>89.6</b> (88.7)	<b>21.1</b> (33.8)	<b>63.3</b> (61.5)	<b>68.0</b> (66.5)	<b>75.0</b> (75.0)	<b>86.0</b> (86.1)	<b>100.0</b> (98.9)	<b>115.0</b> (114.4)	<b>132.2</b> (124.1)
Height, cm	<b>177.9</b> (175.9)	<b>7.7</b> (15.0)	<b>165.0</b> (163.2)	<b>168.0</b> (166.0)	<b>173.0</b> (170.9)	<b>178.0</b> (176.1)	<b>183.0</b> (180.9)	<b>188.0</b> (185.4)	<b>189.2</b> (188.2)
<b>Females (N = 507)</b>									
Weight, kg	<b>77.9</b> (75.4)	<b>22.4</b> (26.8)	<b>52.0</b> (50.2)	<b>54.8</b> (53.6)	<b>62.0</b> (61.1)	<b>72.0</b> (71.3)	<b>88.0</b> (85.5)	<b>109.2</b> (102.2)	<b>123.0</b> (113.8)
Height, cm	<b>163.6</b> (162.1)	<b>7.6</b> (10.8)	<b>152.0</b> (150.7)	<b>154.9</b> (153.1)	<b>158.7</b> (157.3)	<b>163.0</b> (162.1)	<b>168.0</b> (166.8)	<b>173.0</b> (170.9)	<b>177.8</b> (173.7)

68 The in-plane resolution of CT scan images varied between 0.54 mm and 0.98 mm with a median of  
 0.70 mm. CT slice spacing varied between 0.625 mm (16 % of scans) to 5 mm (18 % of scans), with the  
 70 majority (58 %) having slice spacing at 1.25 mm. Demonstration of the relative accuracy of rib centroid  
 position and measurements (described below) taken from these varied scan resolutions is provided as sup-  
 72 plementary material.

### Individual ribs present in scan

74 From the 1042 adult CT scans, a total of 20,204 individual ribs were fully captured within CT scan win-  
 dows. Ribs with fracture were identified based on radiology reports associated with the CT image or visual  
 76 inspection and were excluded from analysis leaving a total of 20,627 included observations. Mid-level ribs

were the most commonly fractured and therefore had a greater exclusion rate than other ribs, however all levels from 2 through 12 retained at least 1600 uninjured ribs as observations.

### **Rib centroid extraction**

Rib centroidal path geometry was extracted for each rib from its corresponding CT scan volume in the form of a series of 3D point coordinates running along its centroidal path (i.e., the sequence of centroids connecting adjacent cross-sections). The extraction process was performed using semi-automated software written in MATLAB, and is described in detail in Holcombe et al.<sup>22</sup> and summarized as follows. Firstly, points are manually placed at the rib's head (the end proximal to the spine, specifically on the articulation point between rib and vertebral body) and the rib end distal to the spine (at the apex of the cup-shaped costochondral junction). The centroidal path is then extracted by building an initial rib path between end points from an algorithm adapted from Staal et al.<sup>25</sup>, followed by iterative refinement of that path by taking cross sectional slices through the CT volume and identifying the 2D centroid of filled regions of segmented rib cortical bone.

### **Rib plane and orientation parameters**

A local rib coordinate system was fitted to each set of centroidal path rib points, having its origin at the rib's proximal end landmark, its local x-axis passing through the distal end landmark, and its local y-axis chosen so as to minimize the distance of all rib points from the local x-y plane. Three rotational parameters then define the orientation of this local rib plane with respect to a fixed body coordinate system as shown in Figure 2.

A rib's pump-handle parameter ( $\alpha_{PH}$ ) is specified as the angle between the rib local x-axis and the coronal plane. A rib's lateral swing ( $\alpha_{LS}$ ) is the angle between the rib local x-axis and the sagittal plane, and its bucket-handle angle ( $\alpha_{BH}$ <sup>17</sup>) is a rotation about the rib's local x-axis after the prior rotations are performed. The convention for  $\alpha_{BH}$  was chosen such that rotation moving the lateral aspect of the rib superiorly results in positive  $\alpha_{BH}$ , while rotation moving the lateral aspect of the rib inferiorly results in negative  $\alpha_{BH}$ .

The combination of these three rotational parameters allows an initial neutrally posed rib (on its correct side yet hanging directly inferiorly) to undergo successive rotations by  $\alpha_{PH}$  (up from the sagittal plane),

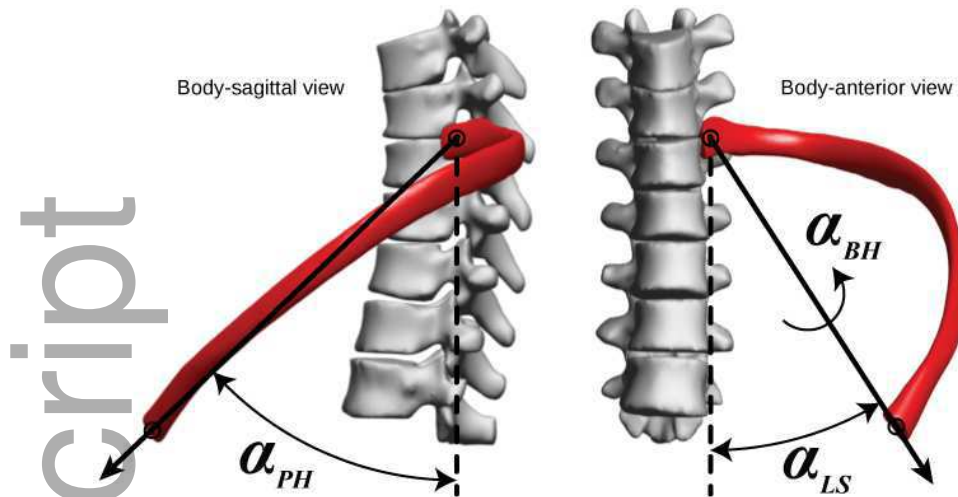


Figure 2: Rib plane parameterisation into pump-handle angle ( $\alpha_{PH}$ ), lateral swing angle off the mid-sagittal plane ( $\alpha_{LS}$ ), and bucket-handle angle ( $\alpha_{BH}$ ).

104  $\alpha_{LS}$  (away from the medial plane), then by  $\alpha_{BH}$  (about the newly rotated x-axis, positive for left-sided ribs and negative for right-sided ribs), with the resulting rib being oriented correctly in the body habitus.

106 To compensate for misalignment between the patient anatomical planes and the global scan coordinate system, a true rib cage lateral vector was created. It is specified as the normal direction to plane of best fit  
 108 through a point cloud consisting of (1) midpoints of all left and right proximal rib end pairs, (2) points at the center of each thoracic vertebrae, and (3) medial points placed along the sternum and *linea alba*. Rib  
 110 plane rotation angles are then defined relative to orthogonal body coronal and sagittal planes derived from this body-lateral vector and the scanning bed.

### 112 Rib in-plane parametric shape model

Each rib's overall shape is characterized using a six-parameter rib shape model introduced in Holcombe  
 114 et al.<sup>22</sup>. Non-linear optimization (performed with MATLAB's Optimization Toolbox) is used to find the set of parameters that minimize the sum-of-squares distance from the original rib points (seen in-plane with  
 116 respect to its local x- and y- axes) to the resulting parameter-based rib model path. A full derivation of rib shape from parameters is described in Holcombe et al.<sup>22</sup>, with the parameters illustrated in Figure 3 and  
 118 their effects summarized below. Individually, the  $S_x$  parameter controls the overall size of a rib by directly prescribing its end-to-end length. The rib's peak is then given by the X-Y pair  $[X_{Pk}, Y_{Pk}]$ , expressed in  
 120 coordinates normalized by  $S_x$ . Consequently,  $1/Y_{Pk}$  describes overall rib aspect ratio in terms of height in



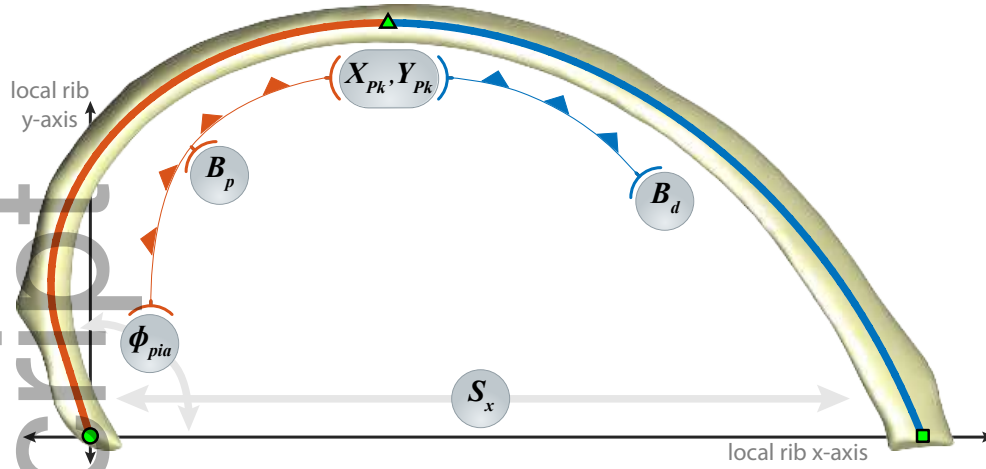


Figure 3: Six-parameter rib model with one size ( $S_x$ ) and five shape parameters. The proximal spiral (from circle to triangle markers) and distal spiral (from triangle to square markers) meet with zero slope at  $[X_{Pk}, Y_{Pk}]$  in normalized rib coordinates, defining rib aspect ratio ( $Y_{Pk}$ ) and skewness ( $X_{Pk}$ ).  $\phi_{pia}$  defines the inner angle between the proximal rib end and the local x-axis, while  $B_p$  and  $B_d$  are proximal and distal spiral constants, respectively.

the local plane versus  $S_x$ , while  $X_{Pk}$  describes “skewness” of the rib’s shape independent of aspect ratio, with a low  $X_{Pk}$  moving the rib peak closer to the proximal end, while larger  $X_{Pk}$  values push this peak towards the distal end. The  $\phi_{pia}$  parameter directly controls the inner angle between the rib’s path and the local x-axis at the proximal end, and  $B_d$  and  $B_p$  are logarithmic spiral constants that modulate the local curvature of the rib in its distal and proximal regions, respectively.

### Derived shape properties

The shape model parameters include four direct geometric measures (size, aspect ratio, skewness, and proximal inner angle) as part of its parameterization. Five additional geometric properties were measured to further quantify key aspects of the resulting rib shapes. Overall arc length in the local plane ( $L_{2d}$ ), overall arc length including out-of-plane deviation ( $L_{3d}$ ), inner angle at the distal end ( $\phi_{dia}$ ), and local curvature at both the distal end ( $\kappa_{dist}$ ) and posterior extension ( $\kappa_{post}$ ) were chosen as additional derived measures, as illustrated in Figure 4.

The equation for the curvature  $\kappa$  at any given location  $\theta$  of a logarithmic spiral has the basic form<sup>26</sup> given in Equation (1) below:

$$\kappa = \frac{e^{-B\theta}}{a\sqrt{1+B^2}} \quad (1)$$

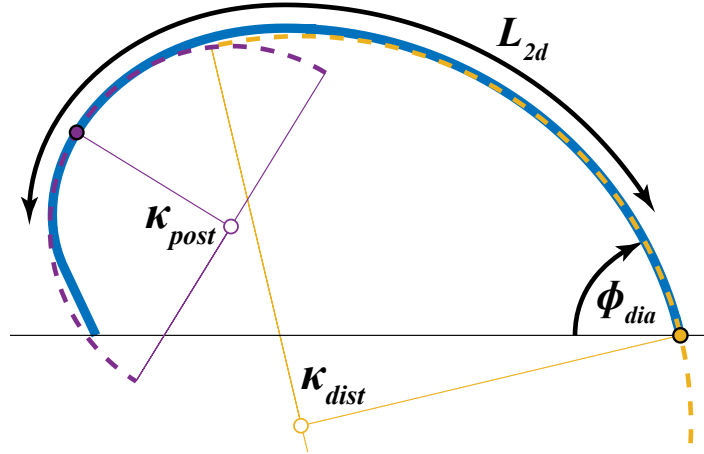


Figure 4: Derived geometric shape measurements of arc length ( $L_{2d}$ , mm), distal inner angle ( $\phi_{dia}$ , deg) and local curvature at the rib posterior and distal end locations ( $\kappa_{post}$ ,  $\kappa_{dist}$ ,  $\text{mm}^{-1}$ ).

where  $B$  is the logarithmic constant ( $B_p$  for the proximal spiral and  $B_d$  for the distal spiral), and where  
 136  $a$  is the scale factor used to transform the unscaled spiral equations from their original  $[x, y]$  space to the local rib plane, given in Holcombe et al.<sup>22</sup>.

138 Substituting those factors along with either  $B_p$  or  $B_d$  into Equation (1) we can interrogate any proximal or distal rib location for its local curvature  $\kappa$  (or its radius of curvature which is  $\frac{1}{\kappa}$ ).

140 The distal curvature is measured at the distal rib end rotational coordinate ( $\theta_{end}$ ). The posterior extension curvature is measured at the rib location furthest from a line drawn between the proximal rib end and the rib  
 142 peak (at  $[X_{Pk}, Y_{Pk}]$ ). This corresponds to a rotational coordinate ( $\theta_{post}$ ) for substitution into Equation (1) of:

$$\theta_{post} = 2 \arctan(\sqrt{B_p^2 + 1} + B_p) \quad (2)$$

## 144 Statistical analysis and methods

Data for this study are presented in two forms. Firstly, scattered data plots showing the overall trends with  
 146 age of each of the rib shape model parameters are given, and are accompanied by simple univariate regression results calculated separately for males and females showing the ability of age and sex alone to predict  
 148 rib shape factors. Secondly, multivariable linear regression is performed, regressing the rib shape parameter values to the demographic factors of age, height, weight, and sex. Coefficients from the multivariable regression analyses quantify the independent effects of each demographic factor on rib shape parameters, and  
 150

are then used to graphically depict the expected variation in rib shapes as these demographic factors change.

152 In all analyses, statistical significance is determined at the  $p < 0.01$  level.

## Results

### 154 Rib shape fit and variation by level

The six-parameter rib shape model was fitted to 20,627 uninjured adult ribs. For in-plane model fitting, 156 the mean absolute error (MAE) between the parameterized model and points on the original geometry was 0.40 mm. Parameter distribution patterns across the rib cage (see Figure A1) matched closely to those originally reported from a smaller population in Holcombe et al.<sup>22</sup>, and the reader is directed to that study for 158 discussion of rib-level trends. The population-wide data for each of the rib shape parameters also followed normal distributions, typified by those shown for 6<sup>th</sup> ribs shown in Figure A2 which also shows inter- 160 parameter correlations, discussed further below.

### 162 Scatter data and trends with age

Overall population results for each of the six rib shape parameters are shown in Figure 5 and for each of the 164 three rib orientation parameters in Figure 6. Fitted linear regression lines to age for males and females are shown on the plots for each rib level and parameter, and the explanatory power (r-squared) of age to explain 166 population variation is included.

The first row of plots in Figure 5 show that there is indeed a significant trend in rib end-to-end span ( $S_x$ ) 168 with age, with both male and female rib ends tending to separate with increasing age ( $p < 0.0001$  for all ribs 1–11). The slope for both sexes at the 6<sup>th</sup> rib level is approximately 2.5 mm/decade, with an r-squared value 170 of 7 % for females and 8 % for males. The second row of scattered data in Figure 5 shows that increasing age is correlated with a decrease in the  $Y_{Pk}$  parameter (i.e., increase in aspect ratio,  $p < 0.0001$  for ribs 1–11). Age alone explains around 20 % of the aspect ratio variation at mid-level ribs in females and 17 % 172 in males. Rib skewness ( $X_{Pk}$ ) also shows strong trends with age for lower-level ribs ( $p < 0.0001$  for ribs 6–11,  $p > 0.01$  for ribs 1–4). As individuals age, rib skewness in these areas tends to increase, with age 174 capable of explaining around 9 % of the population variance in both sexes for the 7<sup>th</sup> rib level. Other rib shape parameters show only marginal univariate trends with age, with a slight increase at upper rib levels in 176  $\phi_{pia}$  ( $p < 0.001$  for ribs 1–8) and decrease in  $B_p$  ( $p < 0.01$  for ribs 3–6).

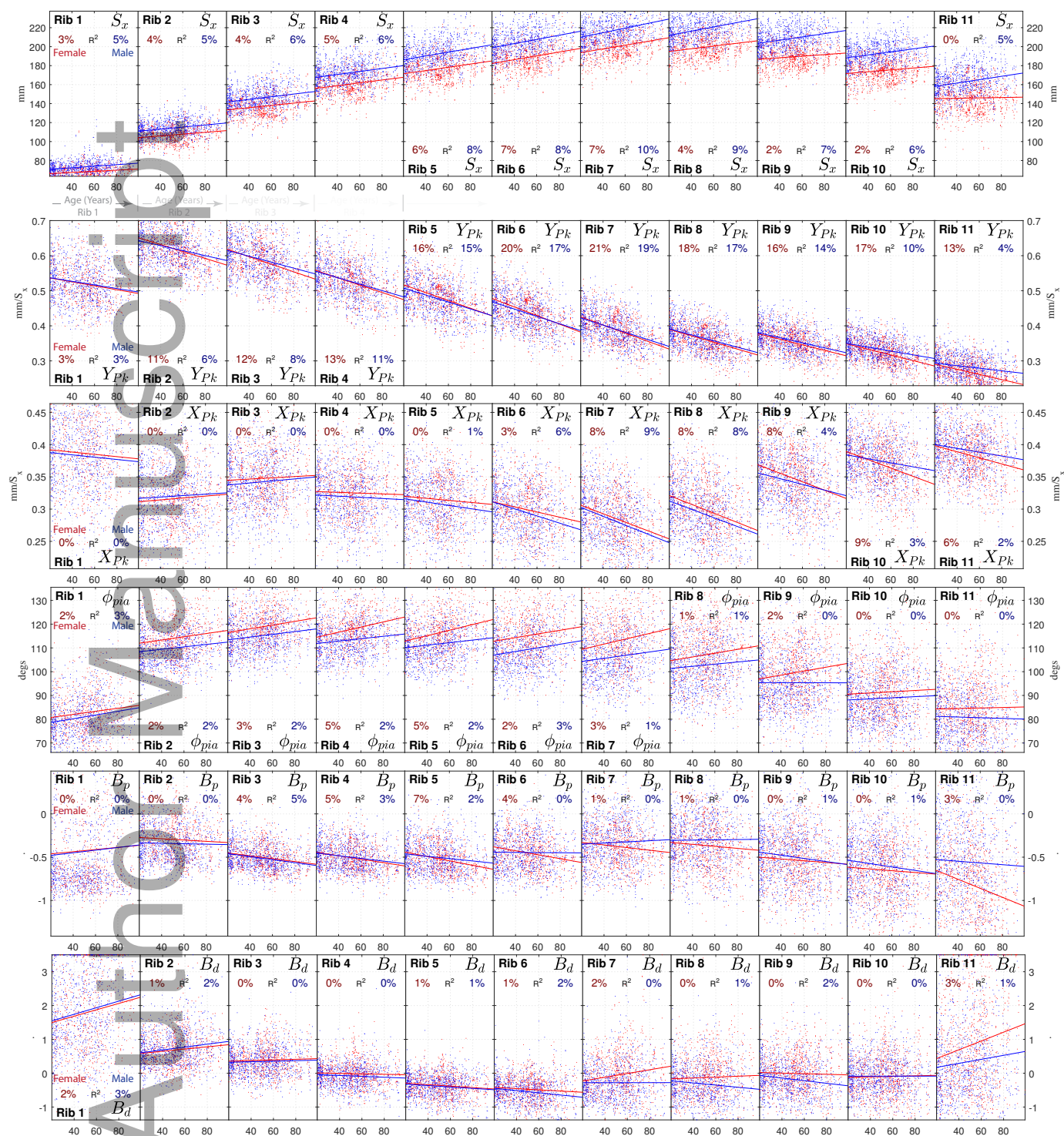


Figure 5: Data point cloud showing all fitted in-plane parameters between ages 20 and 90 years for males (blue) and females (red). Linear regression lines are shown along with their explanatory power (r-squared). Strongest trends with age are seen for rib aspect ratio ( $Y_{Pk}$ ), rib end-to-end length ( $S_x$ ), and rib skewness ( $X_{Pk}$ ) in mid- and lower-level ribs.

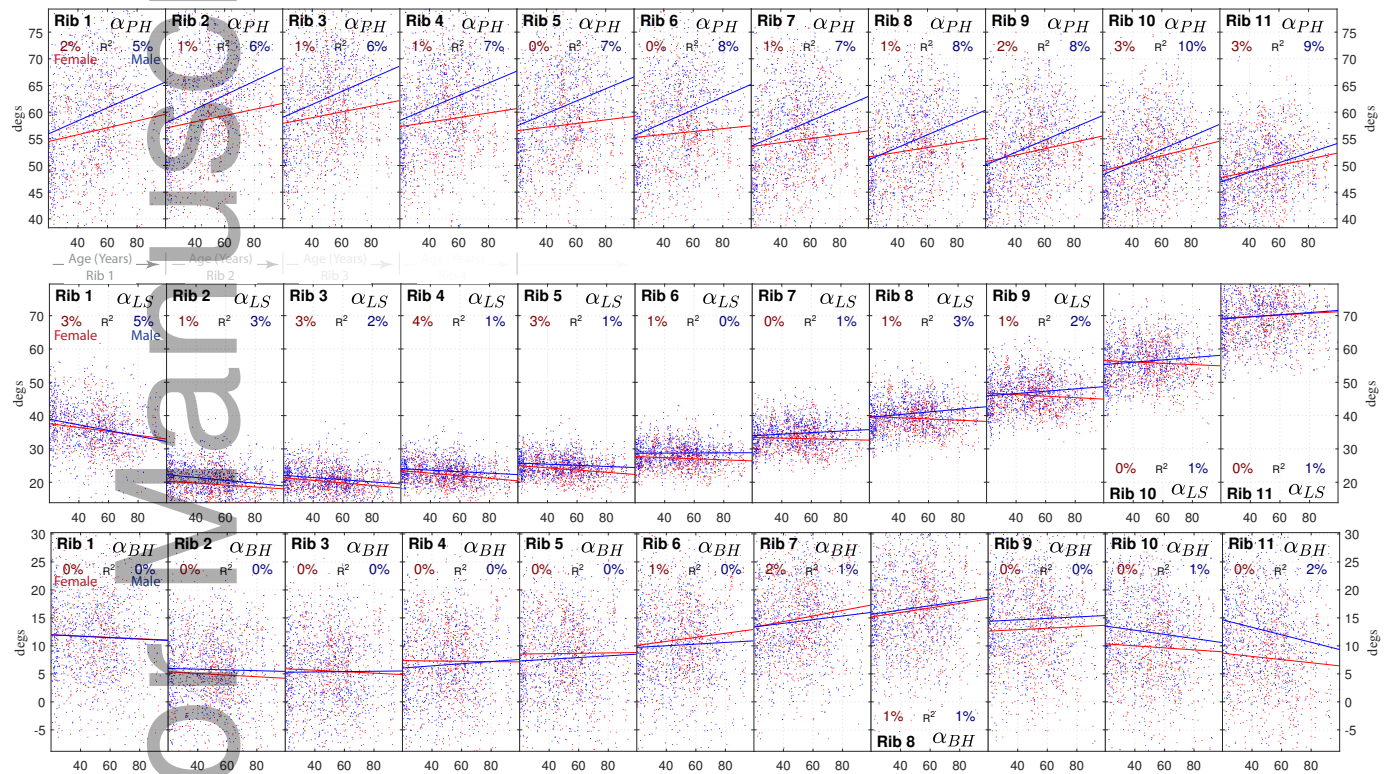


Figure 6: Data point cloud showing all rib pump-handle ( $\alpha_{PH}$ ), lateral swing ( $\alpha_{LS}$ ), and bucket-handle ( $\alpha_{BH}$ ) angle parameters between ages 20 and 90 years for males (blue) and females (red). Linear regression lines are included along with their explanatory power (r-squared).

178 Rib pump-handle  $\alpha_{PH}$  angles are given in Figure 6, with most ribs oriented between  $40^\circ$  (more vertically  
hanging, “narrow-chested”) and  $80^\circ$  (closer to horizontal, “barrel-chested”). Age associations with  $\alpha_{PH}$  are  
180 strongest for males ( $p < 0.0001$  for all male ribs,  $p < 0.01$  for female ribs 1–3 and  $p < 0.001$  ribs 8–11),  
however the rate of change ( $1.43^\circ$  per decade for males at the 6<sup>th</sup> ribs,  $0.43^\circ$  for females) and the percentage  
182 of population variation explained by age alone (8 % within males, none for females) are low.

The lateral swing  $\alpha_{LS}$  parameter shows clear differences by rib level since different ribs extend closer  
184 to the sternum ( $\alpha_{LS}$  near  $20^\circ$ ) in ribs 2 and 3, and finish more laterally with each successive rib level. In  
general only minor univariate trends with age are seen, with increased age associated with slight increases  
186 in  $\alpha_{LS}$  angle for lower ribs in males ( $p < 0.01$ , ribs 7–10). Similarly small univariate aging effect is seen  
in bucket-handle  $\alpha_{BH}$  angles, with age alone unable to explain more than 1 % of the overall population  
188 variance within either sex ( $p > 0.01$  for all except ribs 7 and 8).

### Multivariable regression models

190 The univariate analyses shown in Figures 5 and 6 highlight clear trends in a number of the model parameters  
with age, however they are not necessarily independent of confounding demographic variables such as height  
192 and weight which will also affect rib geometry. Multivariable linear regression was therefore performed for  
each rib and parameter using demographic variables of age, height, weight, and sex as predictors. Full  
194 model regression coefficients for all parameters are supplied in Table A2, while Table 2 gives the proportion  
of population variation within each parameter that is explained by the demographics predictors in each  
196 regression model.

Regression results show, for example, that a person’s height is the most strongly correlated demographic  
198 with rib end-to-end span ( $S_x$ ), and that the 6<sup>th</sup> rib span increases at a rate of 0.54 mm for each gained cm in  
stature ( $p < 0.0001$ ). Similarly, males will have 6<sup>th</sup> ribs  $S_x$  span 10.8 mm longer than females of equivalent  
200 demographics, and the isolated age effect on  $S_x$  is an elongation of 2.5 mm per decade ( $p < 0.0001$ ).

Aspect ratio, on the other hand, is most strongly related to an increase with age, with the peak of the  
202 6<sup>th</sup> rib ( $Y_{Pk}$ ) moving down towards the x-axis in the local rib plane at a rate of 0.01 normalized rib units  
per decade ( $p < 0.0001$ ). Sex and height have negligible influence on  $Y_{Pk}$  values for most ribs, while the  
204 independent effect of weight is to increase aspect ratio at a rate of 0.036 normalized rib units per 10 kg  
gained ( $p < 0.0001$ ).

Table 2: Percentage of overall population variation per parameter explained (r-squared) by regression models to age, height, weight, sex.

#	$S_x$	$X_{Pk}$	$Y_{Pk}$	$\phi_{pia}$	$B_p$	$B_d$	$\alpha_{PH}$	$\alpha_{LS}$	$\alpha_{BH}$
1	23	0	4	4	0	2	30	12	10
2	22	2	8	9	1	2	38	11	1
3	23	5	9	8	6	1	43	10	1
4	28	3	12	10	6	2	45	10	2
5	36	2	16	11	4	1	49	8	3
6	38	4	20	13	1	2	52	6	5
7	39	9	23	13	1	4	52	3	8
8	47	10	22	8	2	5	50	3	13
9	50	9	19	6	1	5	50	2	16
10	49	7	16	5	3	-0	48	3	17
11	35	7	14	3	8	5	41	2	17
12	12	4	4	1	1	0	7	2	8

206 Rib skewness is primarily influenced by age and height, with a movement of the 6<sup>th</sup> rib  $X_{Pk}$  coordinate  
towards the proximal end by about 0.005 normalized rib units per decade and 0.0005 units per cm gained  
208 in stature ( $p < 0.0001$ ).  $\phi_{pia}$  differs significantly by sex, with female 6<sup>th</sup> ribs pointing initially 5.7° more  
posteriorly than male ribs, and a less strong independent age and weight effect also exists, whereby ribs  
210 increase in  $\phi_{pia}$  by around 0.7° per decade and decrease by 0.6° per added 10 kg.

Using the full model parameters presented in Table A2, we can predict the expected set of six shape  
212 parameters per rib for a person of a known demographic, and with those parameters then generate that  
demographic's expected geometric rib shapes. For example, Figure 7 shows the expected geometric rib  
214 shapes determined by the regressed model parameters that are typical for three females and three males of  
50 years of age with heights and weights equal to the CDC 5<sup>th</sup>, 50<sup>th</sup>, and 95<sup>th</sup> percentile height and weight  
216 for their respective sexes (see Table 1).

This same approach is used to illustrate the aging effect on rib shapes in Figure 8. Here, just one stature  
218 demographic is held constant (50<sup>th</sup> percentile female), and person age is varied from 20 to 90 years at 5-year  
increments. From this figure it is clear to see the effect of elongation of the rib span (with the 6<sup>th</sup> rib  $S_x$   
220 progressing from 179 mm to 197 mm) coupled with an increase in overall aspect ratio ( $Y_{Pk}$  shifting from  
0.31 to 0.28 in normalized rib coordinates).

222 Similarly, Figure 9 shows the expected change in rib shapes due to weight. A 50-year-old, 162 cm  
tall female baseline is used, and weight is varied from 40 kg to 175 kg. The results show that rib shape  
224 changes primarily in the mid-to-lower ribs, with expansion of the lateral rib aspects as weight is gained. The

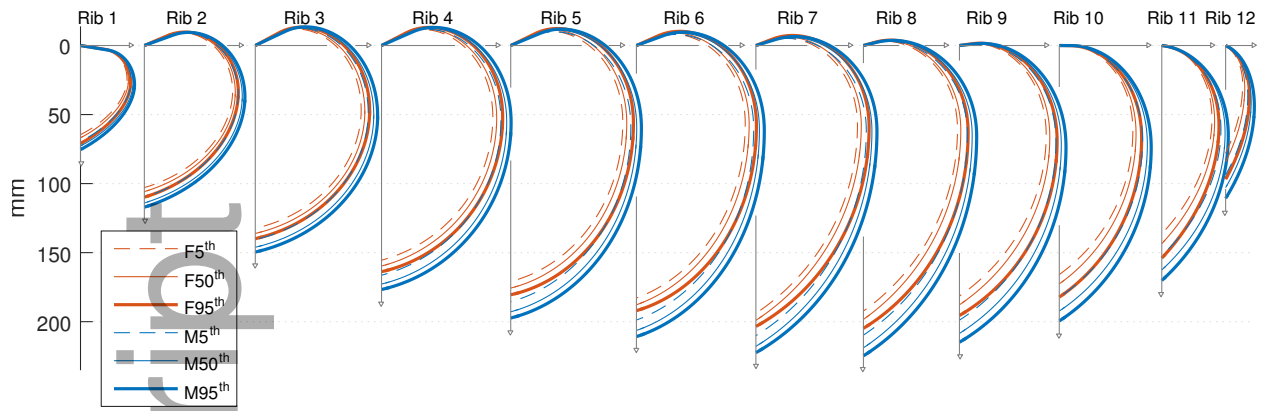


Figure 7: Predicted in-plane rib shapes by demographic for small, medium, and large (CDC 5<sup>th</sup>, 50<sup>th</sup>, and 95<sup>th</sup> percentile weight and stature) males and females, all at 50 years of age.

maximum physical separation between the expected rib shapes for the 40 kg and 175 kg individual in this figure occurs at the antero-lateral region of the 8<sup>th</sup> rib, where the rib paths differ by up to 9 mm in the local rib plane.

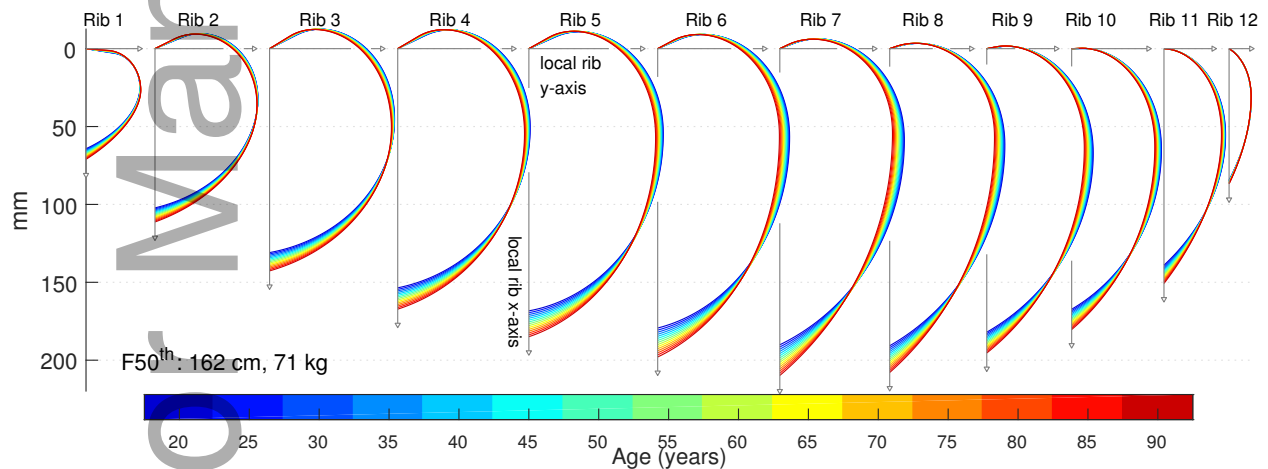


Figure 8: Predicted in-plane rib shapes by age. Baseline demographic is the 50<sup>th</sup> percentile female with specific age represented by line color. Ribs become more elongated and increase in aspect ratio with age.

### 228 Testing model accuracy via indirect parameters

The results seen in Figure 8 show the changes in rib shapes built from sets of shape model parameters that are themselves predicted by regressions to specific demographics (in this case a 50<sup>th</sup> percentile female of various ages). In that sense, all regressed parameters including the direct geometric measures of rib size ( $S_x$ ), aspect ratio ( $Y_{Pk}$ ), skewness  $X_{Pk}$ , and proximal inner angle ( $\phi_{pia}$ ) match the estimated central value for the supplied demographic, at least to the accuracy of the regression models.



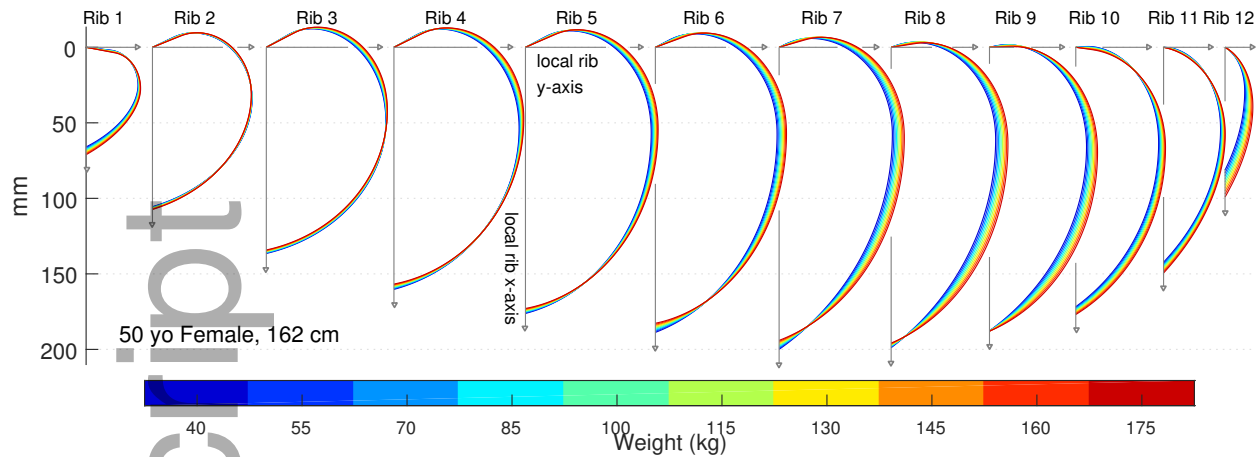


Figure 9: Predicted in-plane rib shapes by weight. Baseline demographic is a 50-years female of 162 cm stature, with specific weight represented by line color. Ribs in heavier individuals are rounder, having lower aspect ratio (higher  $Y_{Pk}$ ).

234 However this does not guarantee that any derived measures of shape (i.e., those not explicitly regressed  
 235 to as model parameters) will also reflect the typical values for a given demographic. For example, the  
 236 inner angle at the distal end ( $\phi_{dia}$ ) is one such rib shape measure which, when measured directly from all  
 237 ribs in the population, is seen to decrease with age ( $p < 0.001$  for all rib levels). The extent to which  
 238 reconstructed rib shapes reflect such trends seen in indirect parameters — when using ribs that are rebuilt  
 239 by sets of predicted parameters with different ages as input to regression — serves to test of the suitability  
 240 of the model presented here to produce geometry that truly reflects overall population trends.

This comparison is illustrated in Figure 10, which shows both expected values (via regression to demo-  
 242 graphics of the values measured directly from ribs in the population) and obtained values (via rebuilt ribs  
 243 using predicted parameter values for that demographic) for each of the four indirect shape measures. The  
 244 displayed demographic series is the 50<sup>th</sup> percentile female, with each observation matching one rib shape  
 245 from the series of F50<sup>th</sup> ribs shown in Figure 8. Corresponding figures for results from small and large  
 246 female and male baseline demographics are given in the Figures A3 to A6.

Results in Figure 10 show that the reconstructed ribs have equivalent length ( $L_{2d}$ ) to the expected rib  
 248 length seen in the population. Trends in inner angle at the distal end ( $\phi_{dia}$ ) and rib curvature at the posterior  
 249 region ( $\kappa_{post}$ ) also match well to the expected population values, with only marginally lower values in  
 250 reconstructed ribs than expected based on measures from the given population. Rib curvature at the distal  
 251 end shows some degree of divergence from population trends, with reconstructed ribs having around 10 %  
 252 lower curvature at this distal extremity than is expected, particularly at the 6<sup>th</sup> rib level in an older population.

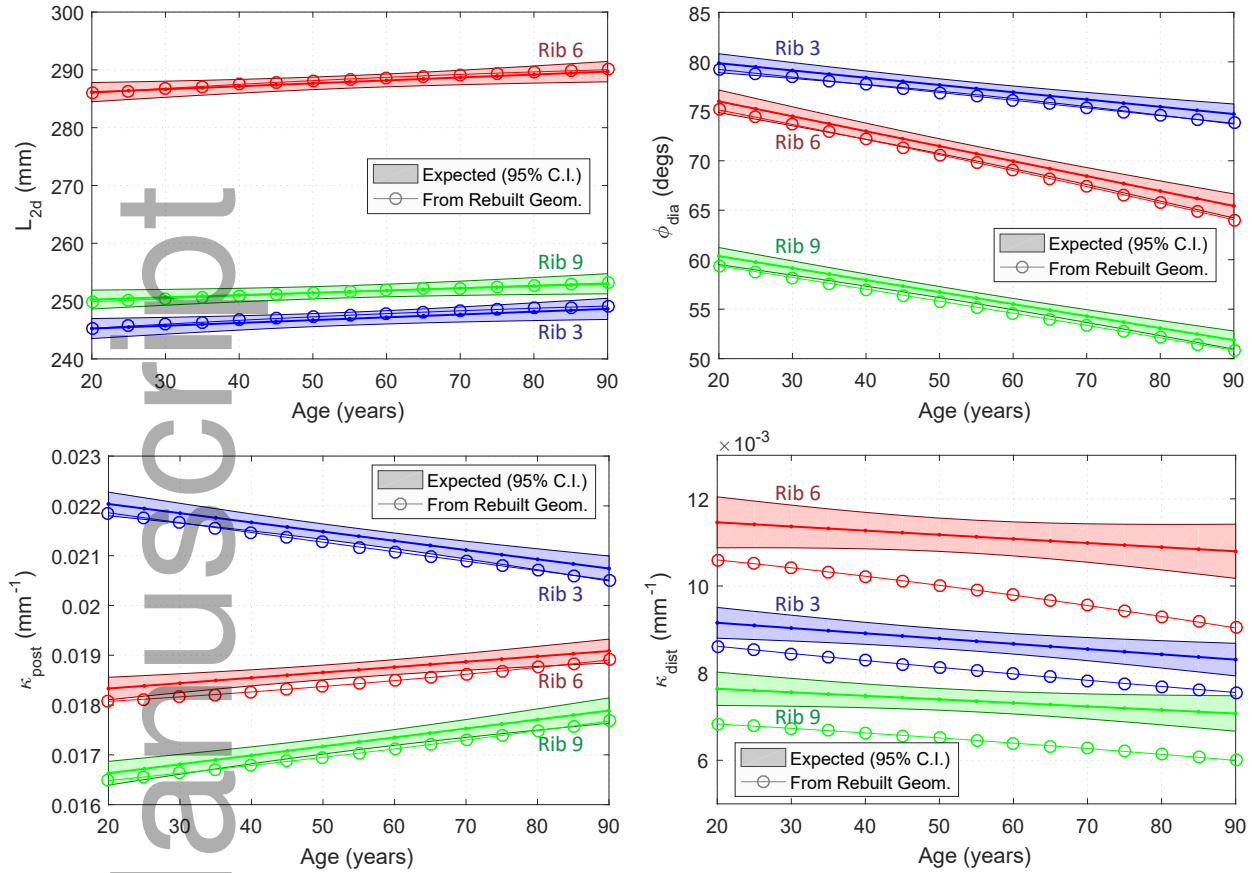


Figure 10: Expected values for rib arc length ( $L_{2d}$ ), inner angle at the distal end ( $\phi_{dia}$ ), and local curvature at posterior ( $\kappa_{post}$ ) and distal ( $\kappa_{dist}$ ) locations, along with values from rebuilt ribs matching that demographic. Regression models fitted to the values measured directly in the population are used to query for the expected values (with 95% confidence interval) for 50<sup>th</sup> percentile females of varying ages.

## Discussion

254 This study has applied parametric models of in-plane rib shape and rib orientation to a large collection of  
 adult rib geometries to characterize the population variation and, in particular, investigate the changes in  
 256 overall rib anatomy that occur with age. Multivariable (age, height, weight, sex) regression models for  
 parameters show significant differences in size, shape, and orientation across demographics and are used to  
 258 produce typical or expected rib shapes for particular demographics. The shape model and regression models  
 are valuable tools for studying age-related anatomic changes and the the associated injuries which may be  
 260 affected by overall rib and rib cage geometry.

## Rib shape model considerations

262 A feature of the shape model introduced in Holcombe et al.<sup>22</sup> and used here is that four of its six parameters  
are themselves inherent geometric measures of rib geometry. This provides an advantage over other gener-  
264 alized methods of rib cage shape analysis such as GPA or PCA – which parameterize the position of a large  
cloud of points – by ensuring that the shape model’s regression coefficients for demographic factors are  
266 themselves directly meaningful and easily understood. For example, the negative coefficients for age in the  
 $Y_{Pk}$  parameter of Table A2 give clear evidence of increasing aspect ratios in ribs throughout adulthood. The  
268 shape model also provides a more concise set of parameters than would otherwise be obtained using point  
cloud data, and results in Figure A2 show that these parameters are each normally distributed across the  
270 population, lending validity to subsequent regression analyses. It should be noted however that most of the  
inter-parameter correlations from Figure A2 are statistically significant ( $p < 0.01$ ). The strongest geometric  
272 correlations are between  $S_x$  and  $Y_{Pk}$  (Pearson’s  $R = 0.64$ ) and  $Y_{Pk}$  and  $X_{Pk}$  ( $R = 0.43$ ) showing that  
ribs with higher aspect ratio (designated by lower  $Y_{Pk}$ ) tend to be longer and also have their peak slightly  
274 shifted towards the middle of the rib (lower skewness). Overall, these correlations indicate that – statisti-  
cally speaking – there might be ways to parameterize rib shapes that are even more efficient than our chosen  
276 6-parameter model, albeit likely at the expense of using parameters with intrinsic geometric meaning.

Another important aspect of the shape model is its accuracy in representing the underlying geometric rib  
278 data. The mean absolute error (MAE) between a target rib point and its fitted shape model was 0.40 mm. For  
comparison to past literature, Kindig’s 7-parameter geometric model based on a circle and a semi-ellipse<sup>20</sup>  
280 reported an MAE of 0.78 mm indicating that, on average, the spiral model used here offers an over 40 %  
reduction in geometric fitting error.

282 Measures of curvature using the shape model from this study showed strong agreement with previously  
published results. Mohr et al.<sup>27</sup> reported average curvature of  $0.017 \text{ mm}^{-1}$  at the posterior regions of  
284 mid-level ribs while Dansereau and Stokes<sup>28</sup> reported maximum curvature along the whole rib between  
 $0.018 \text{ mm}^{-1}$  and  $0.033 \text{ mm}^{-1}$ . In this study the average  $\kappa_{post}$  values for ribs 3-9 fell between  $0.017 \text{ mm}^{-1}$   
286 and  $0.021 \text{ mm}^{-1}$ . At the distal end of the ribs, average  $\kappa_{dist}$  values in this study ranged from  $0.007 \text{ mm}^{-1}$   
to  $0.011 \text{ mm}^{-1}$ , which is similar to the range of  $0.006 \text{ mm}^{-1}$  to  $0.008 \text{ mm}^{-1}$  reported by Mohr et al.<sup>27</sup>.

## 288 Rib changes by demographics

This study attempts to identify specific effects of age on overall rib shape and orientation. Increases in rib  
290 pump-handle  $\alpha_{PH}$  angle were first noted as both a weight effect and an aging effect in males by Kent et al.<sup>9</sup>.  
This age effect has since been confirmed by multiple studies<sup>10,12-14</sup>, albeit with age capable of explaining a  
292 relatively low proportion of the overall population variation in rib angle (4 % and 7 % as reported for males  
by Kent et al.<sup>9</sup> and Weaver et al.<sup>12</sup>, respectively, and with methodology differing across studies). Here we  
294 show similar results, with a positive correlation found between age alone and  $\alpha_{PH}$  capable of explaining  
8 % of male variability and 1 % ( $p < 0.001$ ) of female variability at mid-level ribs. Our multivariable results  
296 show that the inclusion of weight substantially increases this predictive power (r-squared up to 50 % for mid-  
level ribs) and reflect results from Kent et al.<sup>9</sup> whereby weight alone was found to better predict rib angle  
298 than age (r-squared equal to 36 %). These results suggest obesity (or weight gain in general) is strongly  
related to the physical rotation of ribs towards a more horizontal configuration, possibly to accommodate  
300 greater volumes of fat and other soft tissues within the chest and abdominal cavity. Similarly, results also  
show an independent sex effect whereby  $\alpha_{PH}$  rib angles in males are seen to be around 3° more horizontal  
302 than females of equivalent demographics. A reason for this sex difference may come from the differences in  
typical body fat patterns, whereby fat accumulation in males tends to produce relatively higher proportions of  
304 visceral fat (resulting in outward pressure from the abdomen and chest), whereas females tend to accumulate  
higher proportions of subcutaneous fat (which is outside the rib cage and less likely to affect rib angles)<sup>29</sup>.

Beyond results for rib angle, however, a more direct aging effect is highlighted in Figure 8 whereby older  
306 ribs elongate in end-to-end span and adopt a shallower overall curvature, and these changes are reflected in  
the age coefficients for the  $S_x$  and  $Y_{Pk}$  parameters of Table A2. The independent effect of age is to increase  
308 rib  $S_x$  span by up to 2.7 mm (7<sup>th</sup> rib,  $p < 0.001$  for ribs 1–10) for every added decade. As a result, across  
a 70-year adult lifetime an individual of average stature is likely to see the separation between ends of their  
310 longest ribs expand by 2.7 cm, or approximately 13 %. This elongation is coupled with increases in rib  
aspect ratio, with  $Y_{Pk}$  being significantly associated with age for ribs 1–11 ( $p < 0.001$  in ribs 1-10). The  
312 result of this association is that the rib peak moves progressively closer to the x-axis of the local rib plane  
at a rate of between 0.006 (ribs 1 and 10) and 0.01 (mid-level ribs) normalized rib units per decade. For  
314 perspective on these primary aging effects, a 70-year age difference reflects 6<sup>th</sup> rib changes in  $Y_{Pk}$  that  
amount to 1.5 SD from population distributions in  $Y_{Pk}$ , and changes in  $S_x$  that amount to 1.1 SD from  
316

population distributions in  $S_x$ . Each of these shape effects are more strongly associated with age than the  
318 0.8 SD changes seen in  $\alpha_{PH}$ .

Other independent associations with age tend to be less strong and affect a more limited region of the  
320 rib cage. For instance, an age effect on rib skewness is most prominent at mid to lower level ribs (reductions  
in  $X_{Pk}$  of between 0.002 and 0.007 units per decade), whereas age influences  $\phi_{pia}$  angle more prominently  
322 in mid to upper level ribs (increasing by around  $0.7^\circ$  per decade). In the case of  $\phi_{pia}$  there is also a clear  
sex effect, with females having higher  $\phi_{pia}$  angles than males of equivalent demographics by up to  $6.3^\circ$   
324 ( $p < 0.001$ ). Sex is most prominently different in overall rib size, with  $S_x$  seen to be between 2.5 mm  
(1<sup>st</sup> rib) and 10.9 mm (8<sup>th</sup> rib) longer in males than females of equivalent demographics. While these sex  
326 differences occur independently of other demographics and indicate subtle underlying differences between  
female and male rib cage morphology, it should also be recognized that the magnitudes of these differences  
328 are small compared to the individual variability shown for the  $S_x$  and  $\phi_{pia}$  parameters. Person height is  
also strongly correlated with  $S_x$ , with each additional 1 cm in stature corresponding to 0.2 mm to 0.6 mm  
330 extension of  $S_x$  at each rib ( $p < 0.001$ ). Weight is the only demographic variable other than age that is  
independently associated with aspect ratio, in which a small increase is seen in  $Y_{Pk}$  for ribs 4–10 of 0.001  
332 to 0.004 normalized rib units per each added 10 kg. Such changes are consistent with the accumulation of  
body fat within the thorax resulting in increased outward pressure to the rib cage. In general there are few  
334 consistent trends across series of rib levels when considering the  $B_p$  and  $B_d$  spiral constants. Only in  $B_d$  do  
we see decreasing values for ribs 2–11, however these do not meet statistical significance ( $0.03 < p < 0.05$   
336 for ribs 3–6 and 9–11).

Overall, each of the differences that are seen in Table A2 have an accumulated effect to influence rib  
338 shape in multiple ways across demographics as depicted by Figures 7 to 9. It is important to consider that  
each of these figures show only the typical, or statistically central, geometry for each specific demographic  
340 whereas the constituent population itself contains rib geometries exhibiting a much wider range of individ-  
uality. This is reflected by the degree of scatter seen in Figure 5, and by the fact that the explanatory power  
342 (r-squared) of demographics alone to predict rib shape parameters remains below 0.2 for most shape param-  
eters. The particular aging effect of elongation coupled with increased aspect ratio is consistent with Shi  
344 et al.<sup>13</sup>, Wang et al.<sup>14</sup> who reported an increase in the whole rib cage AP depth with age that was associated  
with a decrease in rib cage width especially in the middle of the rib cage. To the best of our knowledge  
346 this is the first study to directly identify these effects as shape changes to the ribs that are independent of

other thoracic changes, and the first to quantify both the shape changes themselves and also the ability of  
348 demographics-based regression to represent the overall population variability.

### Potential mechanisms for age-related shape changes

350 The results for changing rib shape with age were associated ( $p < 0.001$ ) with an in-plane increase in rib arc  
length ( $L_{2d}$ ) as seen in Figure 10. However, when considering the entire rib centroidal length including out-  
352 of-plane deviation ( $L_{3d}$ ), this association with age was no longer present ( $p > 0.4$ ). These results indicate  
that the shape changes identified here do not serve to alter the overall bone length with age, but merely  
354 adjust over time the path that is taken from its proximal to distal end. While it is not the focus of this paper  
to investigate the underlying mechanisms that bring about this change, a number of potential causes can be  
356 identified.

Firstly, increased osteoporosis is a well-documented aging phenomena and, in the spine, this reduction in  
358 bone mineral content leads to deterioration of vertebral support and an associated increase in kyphotic spine  
curvature over time. Osteoporotic bone loss also occurs in ribs and is observed in the form of a progressive  
360 decrease in cortical area with age<sup>30</sup> and an associated increase in intracortical porosity<sup>31</sup>. With the complex  
distribution of material properties and cortical thicknesses across a rib's surface<sup>32</sup>, degradation of bone  
362 materials may lead to altered stress states within the ribs which could serve to gradually modify their overall  
geometric makeup. Given the more advanced rates of osteoporosis seen in women than in men<sup>33</sup>, one might  
364 expect that changes in rib shapes due primarily to the effects of osteoporosis would be similarly accelerated  
in females compared to males. This hypothesis was tested by the addition of an interaction term between  
366 age and sex to the multivariable regression models for the two primary rib shape parameters associated with  
age ( $S_x, Y_{Pk}$ ). The additional interaction term was not significantly different to zero ( $p > 0.01$ ) for any  
368 mid-level ribs and parameters, including those shown to be most strongly associated with age ( $S_x, Y_{Pk}$ ). In  
other words, the age effects on rib shape identified in this study were not found to be significantly different  
370 between males and females, casting doubt on the hypothesis that rib shape changes might come solely from  
the effects of osteoporosis.

372 Another hypothesis comes from an increase in calcification of the costal cartilage that is known to  
occur with age<sup>34–36</sup>. Ribs are connected to the sternum via direct costal cartilage segments (true ribs 1–5)  
374 or indirectly via segments attached to superior cartilage segments (false ribs 6–10), and the presence of

calcification is known to increase the local material and cartilage segment stiffness<sup>37,38</sup>. As the compliance  
376 of the chest is reduced due to calcification of these costal segments, the internal stresses experienced by  
the connecting ribs are likely to change, producing a possible mechanism for changes in overall rib shapes.  
378 Similarly, changes over time to musculature surrounding or attached to the ribs may provide a mechanism for  
altering rib geometry. Sarcopenia (loss of muscle mass) is a well known age-related phenomenon affecting  
380 skeletal muscle, and is also likely to be present in respiratory musculature such as the intercostal muscles  
and diaphragm<sup>39</sup>. This weakening over time of these tissues that offer structural support to the ribs has the  
382 potential to in turn lead to gradual changes in rib bone shape.

### Limitations

384 The resolution of the CT scans used in any medical imaging study poses a limitation on accuracy when  
extracting underlying geometry. For instance, Perz et al.<sup>40</sup> showed that simple thresholding of bone in  
386 cross-sectional views produced significant error when measuring cortical bone cross-sectional area in lower  
resolution clinical CT scans. The shape model investigated here focuses only on the central axis of the  
388 rib and does not attempt to capture cross sectional geometry or other changes in rib cortical surfaces that  
may vary across the population. This is itself a limitation in terms of the results that are reported in this  
390 study, however it also serves to alleviate problems with scan resolution since overall rib cross sections  
(from which the central axis is derived) are structures many times larger than pixel sizes in even the lowest  
392 resolution scans. A sensitivity analysis (provided as supplementary information) across the full range of  
scan resolutions and slice spacing found that the error in absolute position of any given cross sectional data  
394 point in lower resolution scans was  $(0.36 \pm 0.19)$  mm, while the resulting error in geometric shape model  
parameters such as size and aspect ratio was below 0.4 %.

396 The population itself is large compared to previous studies of rib and rib cage shape, with data from  
1042 live subjects. While study demographics match well to the general US population, it should be noted  
398 that subjects are sampled from one region of North America and individual ethnicity was not considered, so  
care should be taken when extending results to different regional populations.

400 The CT scans were taken under a trauma protocol having the patients hold their breath during the image  
capturing sequence, meaning results reported here are for a condition of maximal lung inspiration. It is  
402 expected that some patients may have had difficulty adhering to this protocol, particularly those with chest

injuries, and this could lead to variations in measured rib angle from an otherwise healthy population due to  
404 expected differences throughout a respiratory cycle<sup>41,42</sup>.

Rib pump-handle  $\alpha_{PH}$  angles are reported with respect to the scan coronal plane or scanning bed.  
406 However, spine posture varies throughout the population, and since ribs articulate directly with the spine,  
kyphosis seen in some portions of the elderly population<sup>43</sup> would serve to lower  $\alpha_{PH}$  angles in those  
408 individuals. This difference should be accounted for when comparing the current results to measures of  
independent orientation of ribs with respect to a curved spine rather than a fixed reference plane.

410 The inner organs and other internal anatomy of the chest is asymmetrical, which would in turn lead  
to some degree of asymmetry between left and right sided rib anatomy. Small but statistically significant  
412 differences in  $X_{Pk}$  and  $\phi_{pia}$  parameters across sides were observed, indicating some nominal difference in  
skewness between ribs on the left and right sides of the body. With the goal of this study being to describe  
414 the more substantial variations seen across demographics however, ribs from left and right sides were pooled  
and results reported by rib level only.

416 Finally, results show that some amount of care should be taken when using the demographics-based  
regression model in applications that are strongly dependent on the local curvature at the distal end of the  
418 rib ( $\kappa_{dist}$ ). The regression models for each direct parameter (size, aspect ratio, skewness, inner angle at  
the proximal end) ensure a central estimate is obtained for a given demographic, and results also show that  
420 indirect measures of rib length, distal inner angle, and posterior rib curvature are very well represented when  
recreating ribs from these regressed parameters. However, the indirect property of distal rib curvature ( $\kappa_{dist}$ )  
422 is seen to be slightly underestimated in these recreated rib shapes when compared to the true curvature seen  
directly in the population.

## 424 **Future work and applications**

Key components that drive the biomechanical response of ribs to loading include cross-sectional and cortical  
426 geometry, as well as the out-of-plane deviation of the rib's centroidal path. A natural extension of the six-  
parameter in-plane shape model is to expand parameterization to these components, and — provided that  
428 appropriate data sources are used that can accurately resolve these finer details — apply such measurement to  
a broad population. Future work could then quantify the relative influence of age on the individual geometric  
430 and material components in human ribs and provide necessary data for age-specific models of thoracic



anatomy. Results from this study also have relevance in a number of clinical settings. Data presented here  
432 provides normal quantitative ranges for rib shape that are seen throughout the adult population, and the  
associations between those parameters and lung capacity or other measures of disease state may produce  
434 clinically meaningful metrics in the diagnosis and treatment of thoracic skeleton defects and respiratory  
disease.

## 436 **Conclusions**

A statistical model of the human rib shape and orientation in the body was developed that accounts for  
438 variations by age, height, weight, and sex. The size and shape of ribs were represented using a six-parameter  
shape model which was applied to 1042 subjects, and multivariable regression was used for a predictive  
440 model of typical rib geometry based on demographic factors. All demographic factors had statistically  
significant effects on rib shape and orientation, with height and sex being most strongly associated with  
442 rib size, and weight being most strongly associated with rib pump-handle angle. The primary effect of  
age was on a unique aspect of rib shape, with older ribs being more elongated and having flatter overall  
444 curvature than younger ribs. Study results include a statistical rib shape model that gives the geometric  
basis for building ribs that are typical for any specific demographics group, which can in turn be used to  
446 enhance computational modeling of the thoracic rib cage for injury prevention and, in particular, provide a  
quantitative basis for changing rib shapes by age.

## 448 **Conflict of interest statement**

The authors have no conflict of interest that could influence the work described in this manuscript.

## 450 **References**

- 452 (1) Kent, R.; Woods, W.; Bostrom, O. Fatality risk and the presence of rib fractures. *Annual Proceedings,  
Association for the Advancement of Automotive Medicine* **2008**, *52*, 73–82.
- 454 (2) Lee, W. Y.; Yee, W. Y.; Cameron, P. A.; Bailey, M. J. Road traffic injuries in the elderly. *Emergency  
Medicine Journal : EMJ* **2006**, *23*, 42–46.

- 456 (3) Söderlund, T.; Ikonen, A.; Pyhältö, T.; Handolin, L. Factors associated with in-hospital outcomes in  
594 consecutive patients suffering from severe blunt chest trauma. *Scandinavian Journal of Surgery*  
**2015**, *104*, 115–120.
- 458 (4) Veysi, V.; Nikolaou, V.; Paliobeis, C.; Efstathopoulos, N.; Giannoudis, P. Prevalence of chest trauma,  
associated injuries and mortality: a level I trauma centre experience. *International Orthopaedics* **2009**,  
460 *33*, 1425–1433.
- (5) Galan, G.; Penalver, J.; Paris, F.; Caffarena, J.; Blasco, E.; Borro, J.; Garciazarza, A.; Padilla, J.;  
462 Pastor, J.; Tarrazona, V. Blunt chest injuries in 1696 patients. *European Journal of Cardio-Thoracic*  
*Surgery* **1992**, *6*, 284–287.
- 464 (6) Bonne, S.; Schuerer, D. J. E. Trauma in the Older Adult. *Clinics in Geriatric Medicine* **2013**, *29*,  
137–150.
- 466 (7) Wuermser, L. A.; Achenbach, S. J.; Amin, S.; Khosla, S.; Melton, L. J. What Accounts for Rib Frac-  
tures in Older Adults? *Journal of Osteoporosis* **2011**, *2011*, 1–6.
- 468 (8) Hu, J.; Reed, M. P. Focusing on Vulnerable Populations in Crashes: Recent Advances in Finite Element  
Human Models for Injury Biomechanics Research. *Journal Of Automotive Safety And Energy* **2012**, *3*,  
470 295.
- (9) Kent, R.; Lee, S.-H. H.; Darvish, K.; Wang, S.; Poster, C. S.; Lange, A. W.; Brede, C.; Lange, D.;  
472 Matsuoka, F. Structural and material changes in the aging thorax and their role in crash protection for  
older occupants. *Stapp Car Crash Journal* **2005**, *49*, 231–249.
- 474 (10) Gayzik, F. S.; Yu, M. M.; Danelson, K. A.; Slice, D. E.; Stitzel, J. D. Quantification of age-related shape  
change of the human rib cage through geometric morphometrics. *Journal of Biomechanics* **2008**, *41*,  
476 1545–1554.
- (11) Slice, D. E.; Stitzel, J. Landmark-based geometric morphometrics and the study of allometry. Proceed-  
478 ings of the Society of Automotive Engineers Digital Human Modeling for Design and Engineering  
Symposium. 2004; pp 199–207.

- 480 (12) Weaver, A. A.; Schoell, S. L.; Stitzel, J. D. Morphometric analysis of variation in the ribs with age and sex. *Journal of Anatomy* **2014**, *225*, 246–261.
- 482 (13) Shi, X.; Cao, L.; Reed, M. P.; Rupp, J. D.; Hoff, C. N.; Hu, J. A statistical human rib cage geometry model accounting for variations by age, sex, stature and body mass index. *Journal of Biomechanics*  
484 **2014**, *47*, 2277–2285.
- (14) Wang, Y.; Cao, L.; Bai, Z.; Reed, M. P.; Rupp, J. D.; Hoff, C. N.; Hu, J. A parametric ribcage geometry  
486 model accounting for variations among the adult population. *Journal of Biomechanics* **2016**,
- (15) Kent, R. W.; Crandall, J. R.; Bolton, J.; Prasad, P.; Nusholtz, G.; Mertz, H. The influence of superficial  
488 soft tissues and restraint condition on thoracic skeletal injury prediction. *Stapp Car Crash Journal*  
**2001**, *45*, 183–204.
- 490 (16) Schultz, A. B.; Benson, D. R.; Hirsch, C. Force-deformation properties of human ribs. *Journal of Biomechanics* **1974**, *7*, 303–309.
- 492 (17) Margulies, S. S.; Rodarte, J. R.; Hoffman, E. A. Geometry and kinematics of dog ribs. *Journal of Applied Physiology (Bethesda, Md. : 1985)* **1989**, *67*, 707–712.
- 494 (18) Roberts, S. B.; Chen, P. H. Global geometric characteristics of typical human ribs. *Journal of Biomechanics* **1972**, *5*, 191–201.
- 496 (19) Roberts, S. B. Simple Quantitative Anatomical Model for In-vivo Human Ribs. *Journal of Bioengineering* **1977**, *1*, 443–453.
- 498 (20) Kindig, M. W.; Kent, R. W. Characterization of the centroidal geometry of human ribs. *Journal of Biomechanical Engineering* **2013**, *135*.
- 500 (21) Holcombe, S.; Kindig, M.; Zhang, P.; Parenteau, C.; Rabban, P.; Hully, L.; Wang, S. Age-based predictive model of the pediatric ribcage. *JSAE Transaction* **2013**,
- 502 (22) Holcombe, S. A.; Wang, S. C.; Grotberg, J. B. Modeling female and male rib geometry with logarithmic spirals. *Journal of Biomechanics* **2016**, *49*, 2995–3003.

- 504 (23) Agnew, A. M.; Schafman, M.; Moorhouse, K.; White, S. E.; Kang, Y.-S. The effect of age on the  
structural properties of human ribs. *Journal of the Mechanical Behavior of Biomedical Materials* **2015**,  
506 *41*, 302–314.
- (24) Fryar, C. D.; Gu, Q.; Ogden, C. L. Anthropometric reference data for children and adults: United  
508 States, 2007–2010. *Vital and Health Statistics. Series 11, Data from the National Health Survey* **2012**,  
1–48.
- 510 (25) Staal, J.; van Ginneken, B.; Viergever, M. A. Automatic rib segmentation and labeling in computed  
tomography scans using a general framework for detection, recognition and segmentation of objects in  
512 volumetric data. *Medical Image Analysis* **2007**, *11*, 35–46.
- (26) Weisstein, E. W. Logarithmic Spiral. From MathWorld - A Wolfram Web Resource. [http://](http://mathworld.wolfram.com/LogarithmicSpiral.html)  
514 [mathworld.wolfram.com/LogarithmicSpiral.html](http://mathworld.wolfram.com/LogarithmicSpiral.html), Last visited on 4/4/2016.
- (27) Mohr, M.; Abrams, E.; Engel, C.; Long, W. B.; Bottlang, M. Geometry of human ribs pertinent to  
516 orthopedic chest-wall reconstruction. *Journal of Biomechanics* **2007**, *40*, 1310–1317.
- (28) Dansereau, J.; Stokes, I. A. F. Measurements of the three-dimensional shape of the rib cage. *Journal*  
518 *of Biomechanics* **1988**, *21*, 893–901.
- (29) Enzi, G.; Gasparo, M.; Biondetti, P. R.; Fiore, D.; Semisa, M.; Zurlo, F. Subcutaneous and visceral fat  
520 distribution according to sex, age, and overweight, evaluated by computed tomography. *The American*  
*journal of clinical nutrition* **1986**, *44*, 739–746.
- 522 (30) Pavón, M. V.; Cucina, A.; Tiesler, V. New Formulas to Estimate Age at Death in Maya Populations  
Using Histomorphological Changes in the Fourth Human Rib. *Journal of Forensic Sciences* **2010**, *55*,  
524 473–477.
- (31) Agnew, A. M.; Stout, S. D. Brief communication: Reevaluating osteoporosis in human ribs: The role  
526 of intracortical porosity. *American Journal of Physical Anthropology* **2012**, *148*, 462–466.
- (32) Kemper, A. R.; McNally, C.; Pullins, C. A.; Freeman, L. J.; Duma, S. M.; Rouhana, S. M. The biome-  
528 chanics of human ribs: material and structural properties from dynamic tension and bending tests.  
*Stapp Car Crash Journal* **2007**, *51*, 235–273.

- 530 (33) Cawthon, P. M. Gender Differences in Osteoporosis and Fractures. *Clinical Orthopaedics and Related Research* **2011**, *469*, 1900–1905.
- 532 (34) Navani, S.; Shah, J. R.; Levy, P. S. Determination Of Sex By Costal Cartilage Calcification. *American Journal of Roentgenology* **1970**, *108*, 771–774.
- 534 (35) Semine, A. A.; Damon, A. Costochondral ossification and aging in five populations. *Human Biology* **1975**, *47*, 101–116.
- 536 (36) Stewart, J. H.; McCormick, W. F. A sex- and age-limited ossification pattern in human costal cartilages. *American Journal of Clinical Pathology* **1984**, *81*, 765–769.
- 538 (37) Guo, B.-y.; Liao, D.-h.; Li, X.-y.; Zeng, Y.-j.; Yang, Q.-h. Age and gender related changes in biomechanical properties of healthy human costal cartilage. *Clinical Biomechanics* **2007**, *22*, 292–297.
- 540 (38) Lau, A. G.; Kindig, M. W.; Salzar, R. S.; Kent, R. W. Micromechanical modeling of calcifying human costal cartilage using the generalized method of cells. *Acta Biomaterialia* **2015**, *18*, 226–235.
- 542 (39) Tolep, K.; Kelsen, S. G. Effect of aging on respiratory skeletal muscles. *Clinics In Chest Medicine* **1993**, *14*, 363–378.
- 544 (40) Perz, R.; Toczyski, J.; Subit, D. Variation in the human ribs geometrical properties and mechanical response based on X-ray computed tomography images resolution. *Journal of the Mechanical Behavior of Biomedical Materials* **2015**, *41*, 292–301.
- 548 (41) Bellemare, J.-F.; Cordeau, M.-P.; Leblanc, P.; Bellemare, F. Thoracic Dimensions at Maximum Lung Inflation in Normal Subjects and in Patients With Obstructive and Restrictive Lung Diseases. *Chest* **2001**, *119*, 376–386.
- 550 (42) Bellemare, F.; Jeanneret, A.; Couture, J. Sex differences in thoracic dimensions and configuration. *American Journal of Respiratory and Critical Care Medicine* **2003**, *168*, 305–312.
- 552 (43) Bartynski, W. S.; Heller, M. T.; Grahovac, S. Z.; Rothfus, W. E.; Kurs-Lasky, M. Severe thoracic kyphosis in the older patient in the absence of vertebral fracture: association of extreme curve with age. *American Journal of Neuroradiology* **2005**, *26*, 2077–2085.
- 554

## Appendices

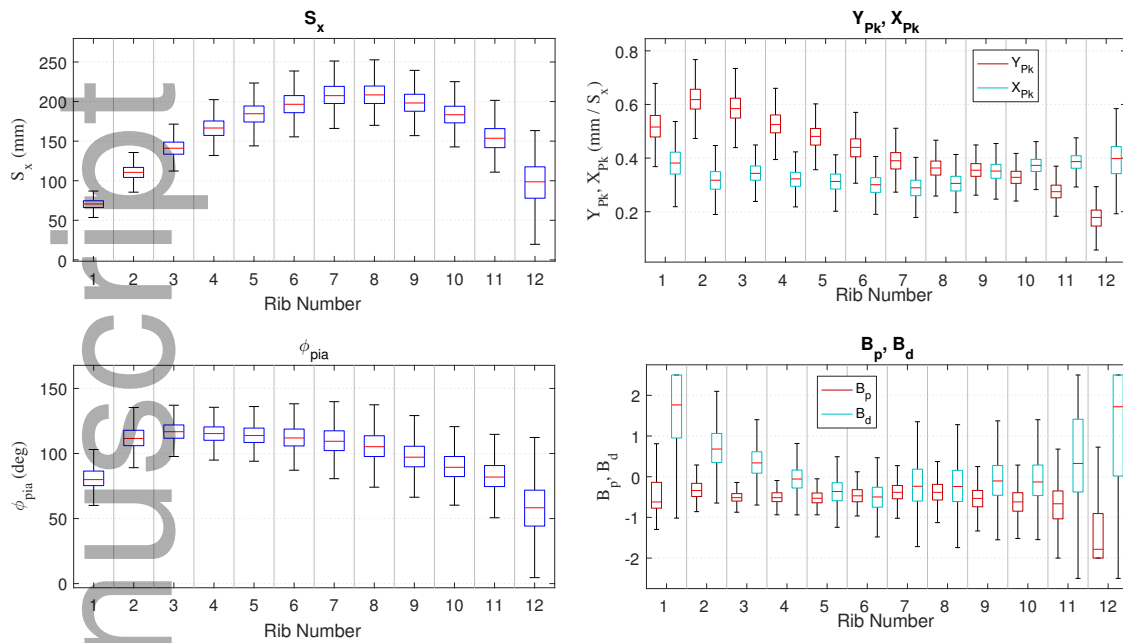


Figure A1: The overall trends in in-plane model parameters across the adult population (N=20,627 ribs). Boxes show the median and the 25<sup>th</sup> to 75<sup>th</sup> quantile ranges and whiskers extend to the  $\pm 2.7\sigma$  range (99.7% coverage).

Table A1: Average  $\pm$  standard deviation in fitted in-plane parameters and rib orientation parameters for all rib levels.

Rib	N	$S_x$ mm	$X_{Pk}$ mm/ $S_x$	$Y_{Pk}$ mm/ $S_x$	$\phi_{pia}$ deg	$B_p$ -	$B_d$ -	$\alpha_{PH}$ deg	$\alpha_{LS}$ deg	$\alpha_{BH}$ deg
1	1444	<b>71.0</b> $\pm 7.2$	<b>0.384</b> $\pm 0.061$	<b>0.521</b> $\pm 0.059$	<b>81.7</b> $\pm 9.3$	<b>-0.43</b> $\pm 0.60$	<b>1.81</b> $\pm 1.16$	<b>58.2</b> $\pm 9.7$	<b>36.2</b> $\pm 7.0$	<b>11.6</b> $\pm 7.4$
2	1665	<b>110.9</b> $\pm 9.6$	<b>0.318</b> $\pm 0.048$	<b>0.621</b> $\pm 0.054$	<b>111.8</b> $\pm 8.6$	<b>-0.32</b> $\pm 0.23$	<b>0.71</b> $\pm 0.55$	<b>60.4</b> $\pm 9.6$	<b>20.3</b> $\pm 4.6$	<b>5.4</b> $\pm 6.9$
3	1681	<b>141.7</b> $\pm 11.9$	<b>0.344</b> $\pm 0.041$	<b>0.588</b> $\pm 0.057$	<b>116.8</b> $\pm 8.3$	<b>-0.51</b> $\pm 0.15$	<b>0.36</b> $\pm 0.42$	<b>61.1</b> $\pm 9.1$	<b>20.7</b> $\pm 3.9$	<b>5.4</b> $\pm 7.0$
4	1661	<b>166.8</b> $\pm 13.7$	<b>0.322</b> $\pm 0.041$	<b>0.527</b> $\pm 0.053$	<b>115.4</b> $\pm 8.5$	<b>-0.50</b> $\pm 0.16$	<b>-0.05</b> $\pm 0.37$	<b>60.3</b> $\pm 8.8$	<b>22.9</b> $\pm 3.6$	<b>6.9</b> $\pm 7.3$
5	1650	<b>184.8</b> $\pm 15.2$	<b>0.312</b> $\pm 0.041$	<b>0.480</b> $\pm 0.050$	<b>113.9</b> $\pm 8.7$	<b>-0.51</b> $\pm 0.18$	<b>-0.37</b> $\pm 0.35$	<b>59.2</b> $\pm 8.7$	<b>24.6</b> $\pm 3.4$	<b>8.2</b> $\pm 7.4$
6	1659	<b>197.3</b> $\pm 16.2$	<b>0.297</b> $\pm 0.042$	<b>0.439</b> $\pm 0.049$	<b>112.0</b> $\pm 9.8$	<b>-0.45</b> $\pm 0.22$	<b>-0.51</b> $\pm 0.40$	<b>57.6</b> $\pm 8.6$	<b>28.0</b> $\pm 3.7$	<b>10.7</b> $\pm 7.3$
7	1714	<b>208.8</b> $\pm 16.3$	<b>0.284</b> $\pm 0.043$	<b>0.391</b> $\pm 0.045$	<b>109.3</b> $\pm 11.3$	<b>-0.35</b> $\pm 0.26$	<b>-0.17</b> $\pm 0.66$	<b>55.9</b> $\pm 8.3$	<b>33.9</b> $\pm 4.3$	<b>14.6</b> $\pm 7.2$
8	1780	<b>209.1</b> $\pm 16.0$	<b>0.297</b> $\pm 0.043$	<b>0.364</b> $\pm 0.039$	<b>104.8</b> $\pm 11.4$	<b>-0.33</b> $\pm 0.29$	<b>-0.22</b> $\pm 0.64$	<b>53.7</b> $\pm 8.0$	<b>39.9</b> $\pm 4.8$	<b>16.6</b> $\pm 7.5$
9	1863	<b>199.0</b> $\pm 15.4$	<b>0.346</b> $\pm 0.041$	<b>0.356</b> $\pm 0.037$	<b>97.4</b> $\pm 11.4$	<b>-0.51</b> $\pm 0.31$	<b>-0.09</b> $\pm 0.59$	<b>53.0</b> $\pm 7.6$	<b>46.5</b> $\pm 5.3$	<b>14.0</b> $\pm 7.6$
10	1905	<b>183.7</b> $\pm 15.1$	<b>0.372</b> $\pm 0.037$	<b>0.329</b> $\pm 0.035$	<b>90.0</b> $\pm 11.3$	<b>-0.62</b> $\pm 0.35$	<b>-0.09</b> $\pm 0.61$	<b>51.4</b> $\pm 7.0$	<b>56.1</b> $\pm 6.4$	<b>11.2</b> $\pm 7.9$
11	1850	<b>154.2</b> $\pm 17.4$	<b>0.388</b> $\pm 0.036$	<b>0.275</b> $\pm 0.036$	<b>82.7</b> $\pm 12.9$	<b>-0.69</b> $\pm 0.56$	<b>0.59</b> $\pm 1.37$	<b>49.4</b> $\pm 5.9$	<b>69.9</b> $\pm 7.6$	<b>10.4</b> $\pm 9.0$
12	1755	<b>95.7</b> $\pm 29.1$	<b>0.390</b> $\pm 0.101$	<b>0.174</b> $\pm 0.045$	<b>60.9</b> $\pm 25.5$	<b>-1.29</b> $\pm 1.66$	<b>1.37</b> $\pm 2.17$	<b>53.3</b> $\pm 8.5$	<b>94.0</b> $\pm 12.0$	<b>14.6</b> $\pm 17.9$

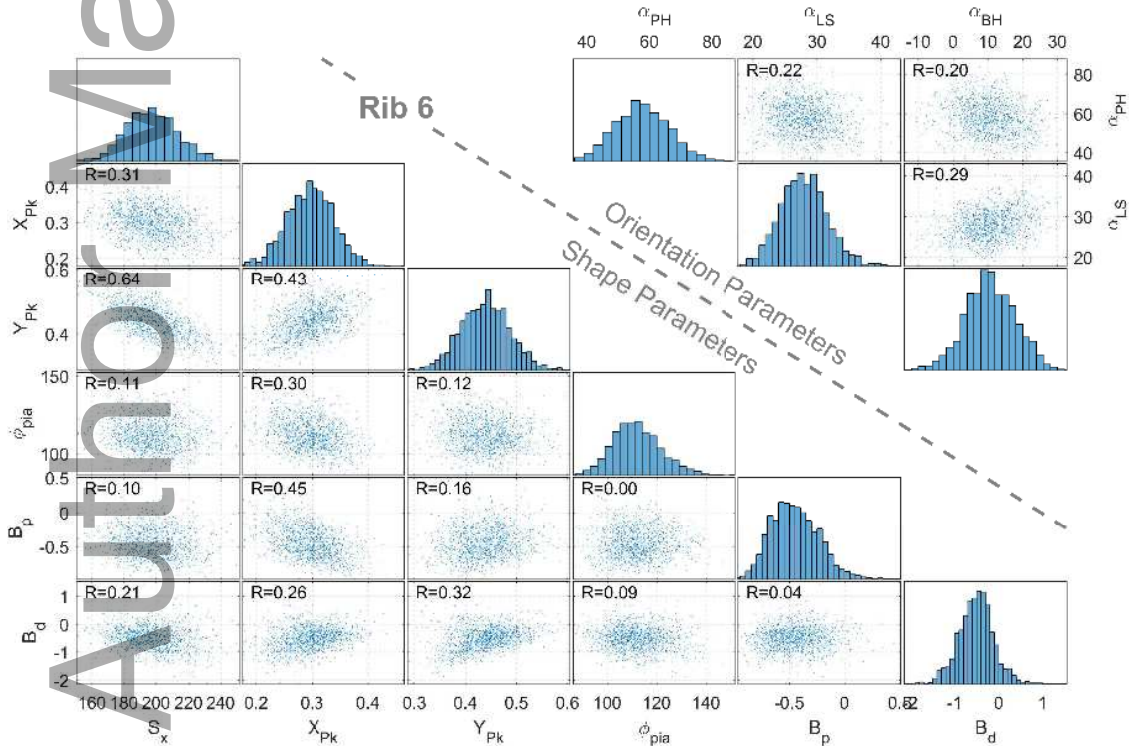


Figure A2: Individual parameter histograms (main diagonal) and inter-parameter correlation plots for the 6<sup>th</sup> ribs. Histograms show parameter distributions in the population to be largely normal. While statistically significant for all pairs except  $B_p$  vs.  $\phi_{pia}$  and  $B_p$  vs.  $B_d$ , inter-parameter correlations (Pearson's R) are low for most parameter combinations, with the strongest between rib size ( $S_x$ ) and aspect ratio ( $Y_{Pk}$ ).

Table A2: In-plane rib shape model with parameter coefficients predicted by demographics. Age (A) is in years, sex (S) is 0 for males and 1 for females, height (H) is in meters, weight (W) is in kilograms, along with the regression intercept (I). Subscript denotes scale factor. For example,  $W_{E-3}$  indicates weight in kg scaled by  $1 \times 10^{-3}$ . Coefficients significantly different from zero at the  $p < 0.01$  level are shown in bold.

#	$S_x$					$X_{Pk}$					$Y_{Pk}$				
	I	A <sub>E-3</sub>	S <sub>E-1</sub>	H <sub>E-1</sub>	W <sub>E-3</sub>	I <sub>E-3</sub>	A <sub>E-5</sub>	S <sub>E-3</sub>	H <sub>E-3</sub>	W <sub>E-5</sub>	I <sub>E-2</sub>	A <sub>E-5</sub>	S <sub>E-3</sub>	H <sub>E-3</sub>	W <sub>E-5</sub>
1	<b>31</b>	<b>98</b>	<b>-24</b>	<b>190</b>	<b>40</b>	<b>415</b>	-23	4	-17	8	<b>62</b>	<b>-63</b>	-9	-36	-7
2	<b>56</b>	<b>129</b>	<b>-34</b>	<b>286</b>	13	<b>292</b>	16	-3	26	<b>-30</b>	<b>67</b>	<b>-83</b>	0	2	-7
3	<b>67</b>	<b>168</b>	<b>-39</b>	<b>403</b>	-9	<b>296</b>	<b>17</b>	7	<b>42</b>	<b>-42</b>	<b>63</b>	<b>-93</b>	-1	-2	13
4	<b>81</b>	<b>195</b>	<b>-61</b>	<b>469</b>	-18	<b>349</b>	-6	4	-0	<b>-31</b>	<b>57</b>	<b>-96</b>	1	-8	<b>24</b>
5	<b>88</b>	<b>237</b>	<b>-90</b>	<b>528</b>	-15	<b>398</b>	<b>-23</b>	2	<b>-39</b>	-11	<b>53</b>	<b>-104</b>	7	-17	<b>27</b>
6	<b>96</b>	<b>265</b>	<b>-102</b>	<b>562</b>	-37	<b>407</b>	<b>-48</b>	-1	<b>-54</b>	8	<b>49</b>	<b>-111</b>	6	-20	<b>37</b>
7	<b>106</b>	<b>283</b>	<b>-105</b>	<b>566</b>	-33	<b>437</b>	<b>-71</b>	-4	<b>-76</b>	<b>18</b>	<b>44</b>	<b>-109</b>	2	-16	<b>39</b>
8	<b>92</b>	<b>246</b>	<b>-106</b>	<b>651</b>	-14	<b>479</b>	<b>-74</b>	-2	<b>-94</b>	<b>20</b>	<b>45</b>	<b>-92</b>	-5	<b>-40</b>	<b>35</b>
9	<b>83</b>	<b>192</b>	<b>-104</b>	<b>648</b>	14	<b>481</b>	<b>-63</b>	1	<b>-70</b>	<b>18</b>	<b>41</b>	<b>-79</b>	-4	-24	<b>29</b>
10	<b>67</b>	<b>187</b>	<b>-93</b>	<b>628</b>	<b>55</b>	<b>467</b>	<b>-52</b>	<b>-8</b>	<b>-41</b>	7	<b>38</b>	<b>-70</b>	<b>-9</b>	-14	<b>11</b>
11	<b>38</b>	<b>168</b>	<b>-85</b>	<b>629</b>	<b>59</b>	<b>524</b>	<b>-48</b>	<b>-14</b>	<b>-62</b>	-0	<b>32</b>	<b>-57</b>	<b>-15</b>	-10	5
12	8	35	<b>-92</b>	<b>469</b>	<b>129</b>	<b>451</b>	<b>-48</b>	<b>-30</b>	-30	<b>33</b>	<b>10</b>	-7	-5	<b>42</b>	<b>15</b>

#	$\phi_{pia}$					$B_p$					$B_d$				
	I	A <sub>E-3</sub>	S <sub>E-1</sub>	H <sub>E-1</sub>	W <sub>E-3</sub>	I <sub>E-2</sub>	A <sub>E-4</sub>	S <sub>E-2</sub>	H <sub>E-2</sub>	W <sub>E-4</sub>	I <sub>E-2</sub>	A <sub>E-4</sub>	S <sub>E-2</sub>	H <sub>E-2</sub>	W <sub>E-4</sub>
1	<b>83</b>	<b>71</b>	10	-12	<b>-34</b>	-85	15	4	23	-8	165	<b>92</b>	-4	-28	22
2	<b>118</b>	<b>62</b>	<b>30</b>	-42	<b>-40</b>	<b>-48</b>	-5	<b>6</b>	9	-0	-5	<b>38</b>	-0	42	<b>-18</b>
3	<b>114</b>	<b>71</b>	<b>32</b>	-1	<b>-27</b>	<b>-28</b>	<b>-17</b>	0	-12	<b>9</b>	-22	10	6	37	<b>-15</b>
4	<b>110</b>	<b>78</b>	<b>41</b>	12	-23	<b>-32</b>	<b>-18</b>	-1	-12	<b>13</b>	50	-11	2	-22	<b>-14</b>
5	<b>100</b>	<b>83</b>	<b>48</b>	63	<b>-36</b>	<b>-34</b>	<b>-19</b>	-2	-6	4	23	<b>-22</b>	-1	-28	-3
6	<b>98</b>	<b>76</b>	<b>59</b>	73	<b>-65</b>	-23	<b>-13</b>	-2	-8	-2	12	<b>-27</b>	4	-27	-7
7	<b>95</b>	<b>81</b>	<b>66</b>	81	<b>-79</b>	<b>-43</b>	-3	-4	10	-7	-31	22	<b>19</b>	13	<b>-34</b>
8	<b>84</b>	<b>69</b>	<b>50</b>	<b>135</b>	<b>-94</b>	<b>-67</b>	-3	-5	26	-7	10	-4	<b>16</b>	1	<b>-47</b>
9	<b>80</b>	<b>42</b>	<b>47</b>	<b>123</b>	<b>-91</b>	<b>-55</b>	<b>-12</b>	-4	7	-1	65	<b>-29</b>	<b>13</b>	-19	<b>-40</b>
10	<b>69</b>	29	<b>32</b>	<b>154</b>	<b>-100</b>	-2	<b>-18</b>	<b>-9</b>	<b>-37</b>	<b>19</b>	32	2	-4	-19	-9
11	<b>66</b>	6	<b>40</b>	<b>126</b>	<b>-84</b>	-53	<b>-29</b>	<b>-22</b>	-14	<b>38</b>	<b>207</b>	<b>81</b>	<b>31</b>	<b>-134</b>	30
12	40	-52	-10	148	-5	-140	<b>65</b>	27	-7	-25	119	4	25	-22	50

#	$\alpha_{PH}$					$\alpha_{LS}$					$\alpha_{BH}$				
	I <sub>E-1</sub>	A <sub>E-3</sub>	S <sub>E-2</sub>	H <sub>E-1</sub>	W <sub>E-3</sub>	I	A <sub>E-3</sub>	S <sub>E-2</sub>	H <sub>E-1</sub>	W <sub>E-3</sub>	I <sub>E-1</sub>	A <sub>E-3</sub>	S <sub>E-1</sub>	H <sub>E-1</sub>	W <sub>E-3</sub>
1	<b>756</b>	<b>96</b>	<b>-358</b>	<b>-236</b>	<b>235</b>	<b>32</b>	<b>-76</b>	-26	<b>95</b>	<b>-92</b>	89	-18	-3	<b>77</b>	<b>-113</b>
2	<b>757</b>	<b>103</b>	<b>-350</b>	<b>-238</b>	<b>263</b>	<b>15</b>	<b>-33</b>	<b>-124</b>	<b>69</b>	<b>-52</b>	87	-7	-12	-1	<b>-25</b>
3	<b>770</b>	<b>94</b>	<b>-350</b>	<b>-243</b>	<b>271</b>	<b>19</b>	<b>-33</b>	<b>-80</b>	<b>47</b>	<b>-47</b>	62	-0	-2	13	<b>-35</b>
4	<b>752</b>	<b>88</b>	<b>-354</b>	<b>-235</b>	<b>272</b>	<b>24</b>	<b>-28</b>	<b>-121</b>	23	<b>-40</b>	93	12	1	6	<b>-48</b>
5	<b>740</b>	<b>86</b>	<b>-357</b>	<b>-235</b>	<b>274</b>	<b>30</b>	<b>-24</b>	<b>-161</b>	-3	<b>-27</b>	89	14	4	18	<b>-54</b>
6	<b>702</b>	<b>87</b>	<b>-318</b>	<b>-227</b>	<b>280</b>	<b>35</b>	-6	<b>-209</b>	-27	<b>-15</b>	107	<b>30</b>	4	25	<b>-70</b>
7	<b>706</b>	<b>88</b>	<b>-266</b>	<b>-236</b>	<b>271</b>	<b>41</b>	8	<b>-205</b>	-34	-6	90	<b>47</b>	1	<b>63</b>	<b>-88</b>
8	<b>664</b>	<b>85</b>	<b>-175</b>	<b>-222</b>	<b>261</b>	<b>46</b>	15	<b>-203</b>	-36	1	98	<b>54</b>	-9	<b>85</b>	<b>-119</b>
9	<b>670</b>	<b>91</b>	<b>-128</b>	<b>-224</b>	<b>243</b>	<b>57</b>	9	<b>-166</b>	<b>-65</b>	15	75	<b>28</b>	<b>-23</b>	<b>103</b>	<b>-136</b>
10	<b>601</b>	<b>102</b>	-78	<b>-182</b>	<b>210</b>	<b>70</b>	10	<b>-126</b>	<b>-101</b>	<b>45</b>	86	-18	<b>-31</b>	<b>95</b>	<b>-133</b>
11	<b>544</b>	<b>77</b>	-16	<b>-132</b>	<b>164</b>	<b>83</b>	25	-76	<b>-103</b>	<b>40</b>	65	<b>-34</b>	<b>-48</b>	<b>107</b>	<b>-123</b>
12	<b>631</b>	<b>49</b>	-113	<b>-117</b>	<b>96</b>	<b>116</b>	35	-81	<b>-113</b>	<b>-44</b>	146	-9	<b>-72</b>	101	<b>-160</b>



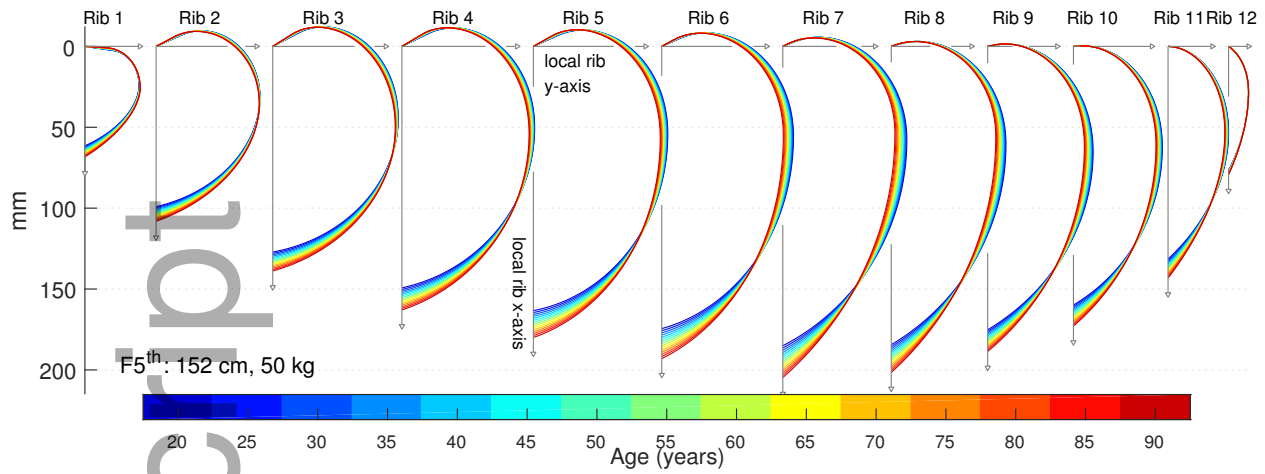


Figure A3: Predicted in-plane rib shapes by age. Baseline demographic is the 5<sup>th</sup> percentile female with specific age represented by line color. Ribs become more elongated and increase in aspect ratio with age.

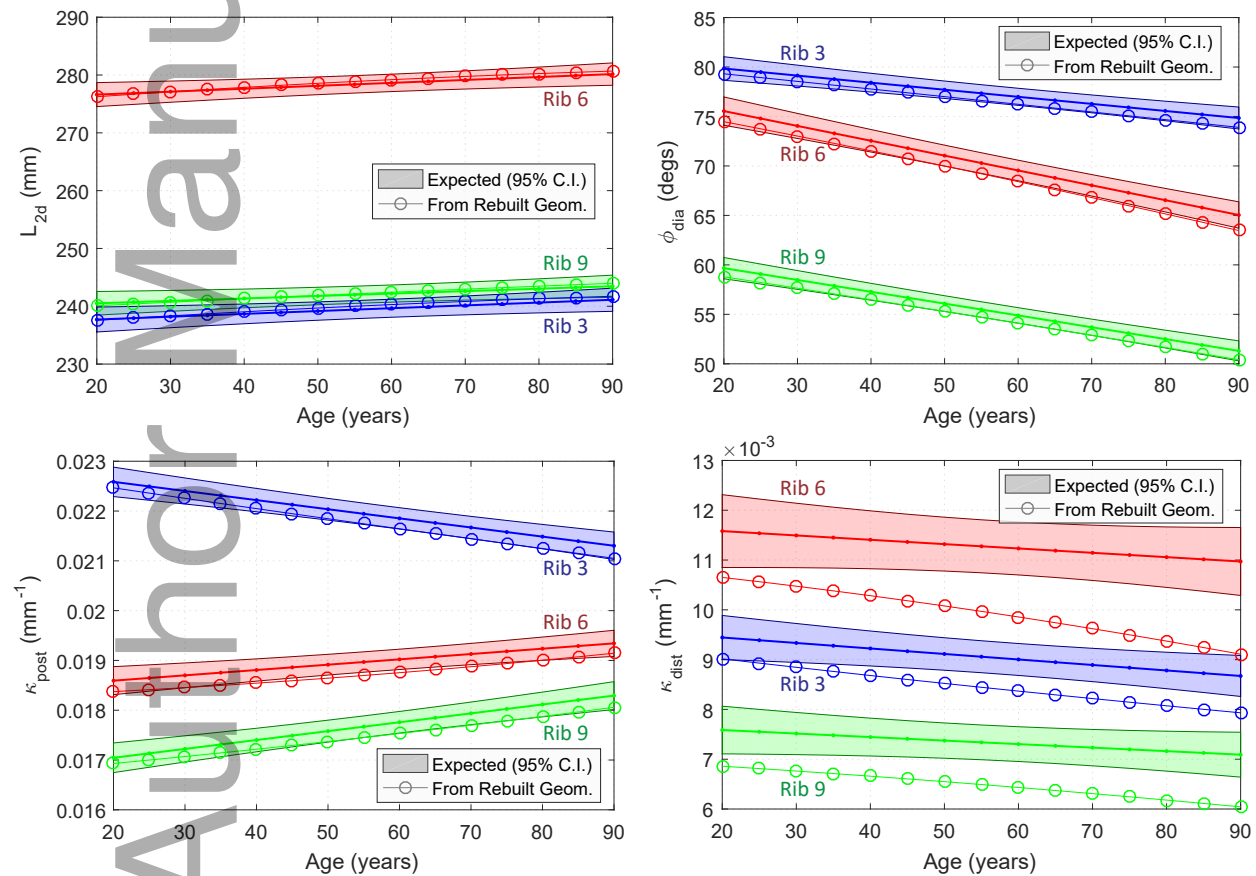


Figure A4: Expected values for rib arc length ( $L_{2d}$ ), inner angle at the distal end ( $\phi_{dia}$ ), and local curvature at posterior ( $\kappa_{post}$ ) and distal ( $\kappa_{dist}$ ) locations, along with values from rebuilt ribs matching that demographic. Regression models fitted to the values measured directly in the population are used to query for the expected values (with 95% confidence interval) for 5<sup>th</sup> percentile females of varying ages.

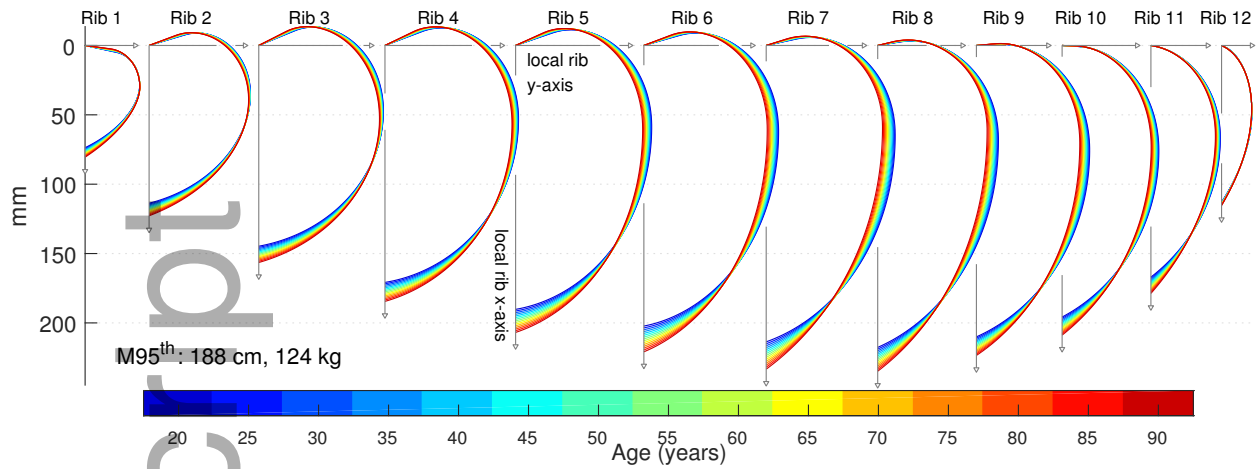


Figure A5: Predicted in-plane rib shapes by age. Baseline demographic is the 95<sup>th</sup> percentile male with specific age represented by line color. Ribs become more elongated and increase in aspect ratio with age.

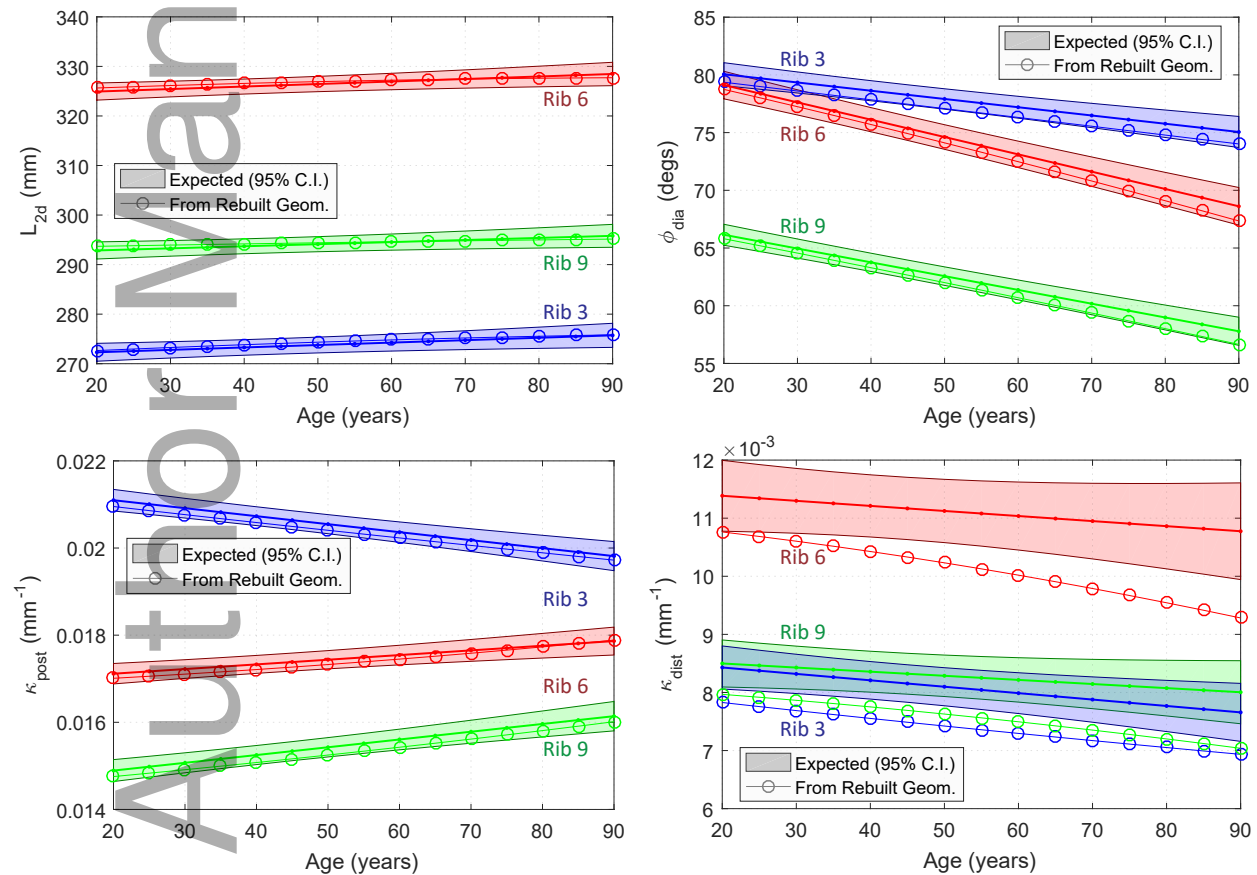
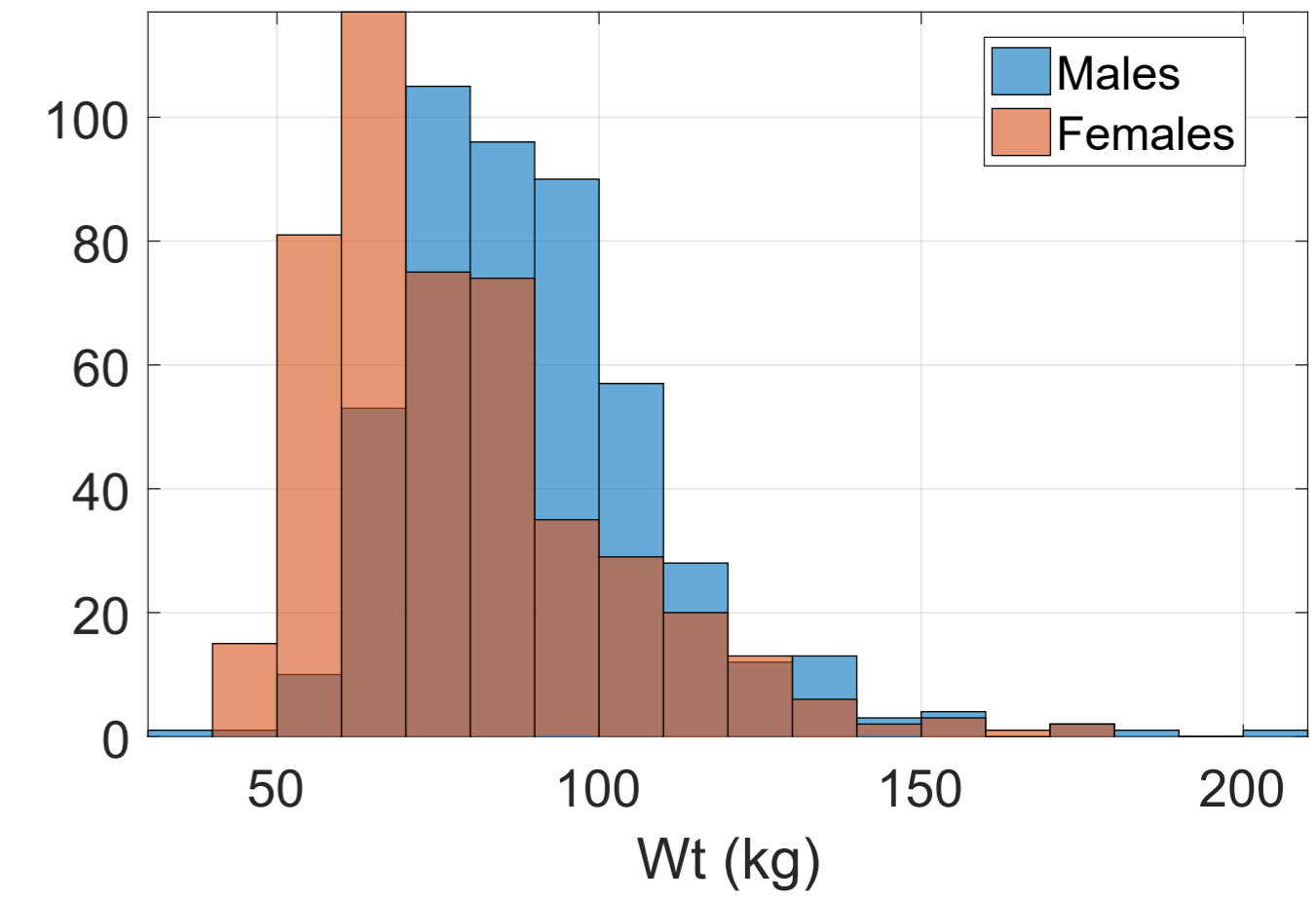
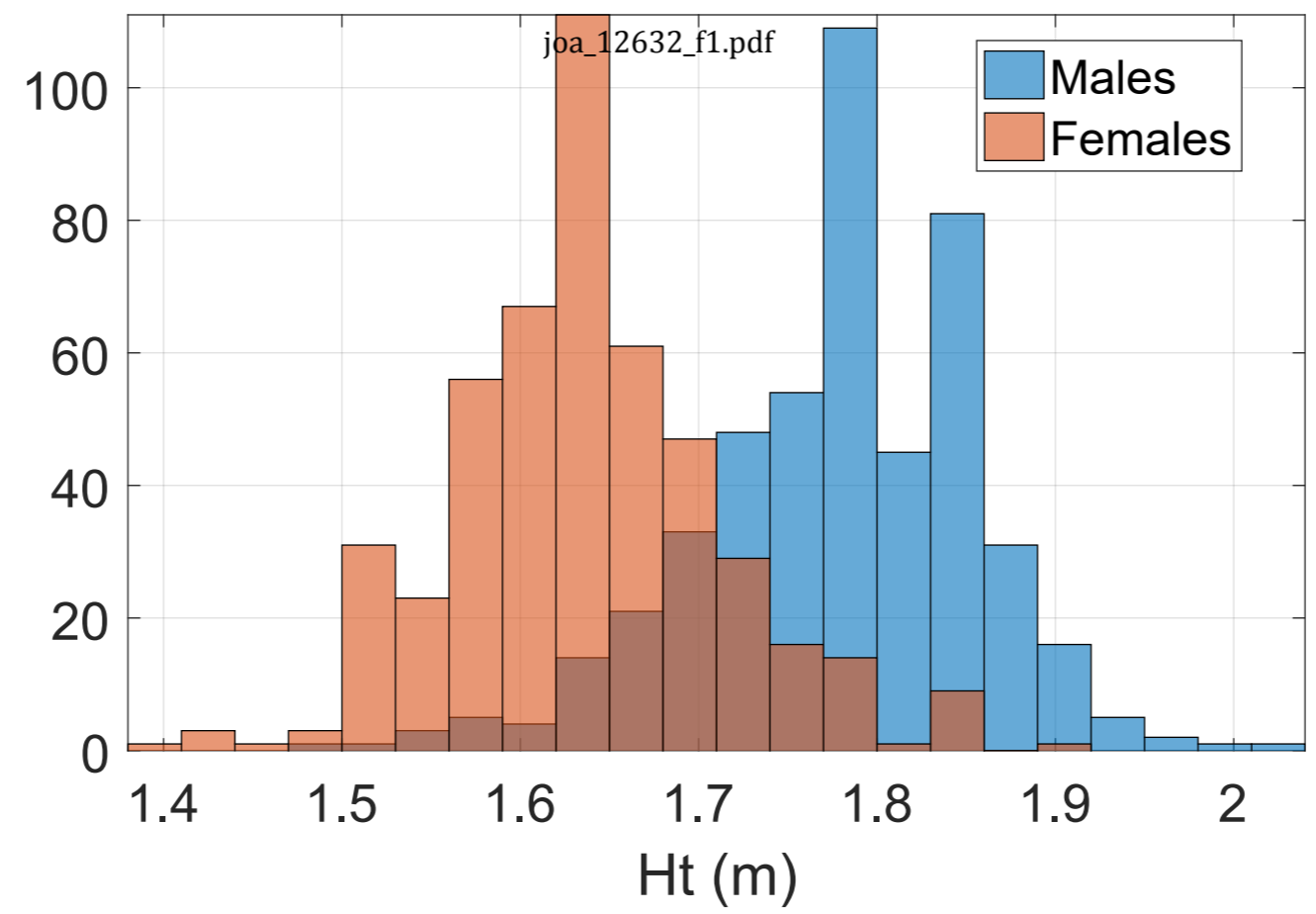
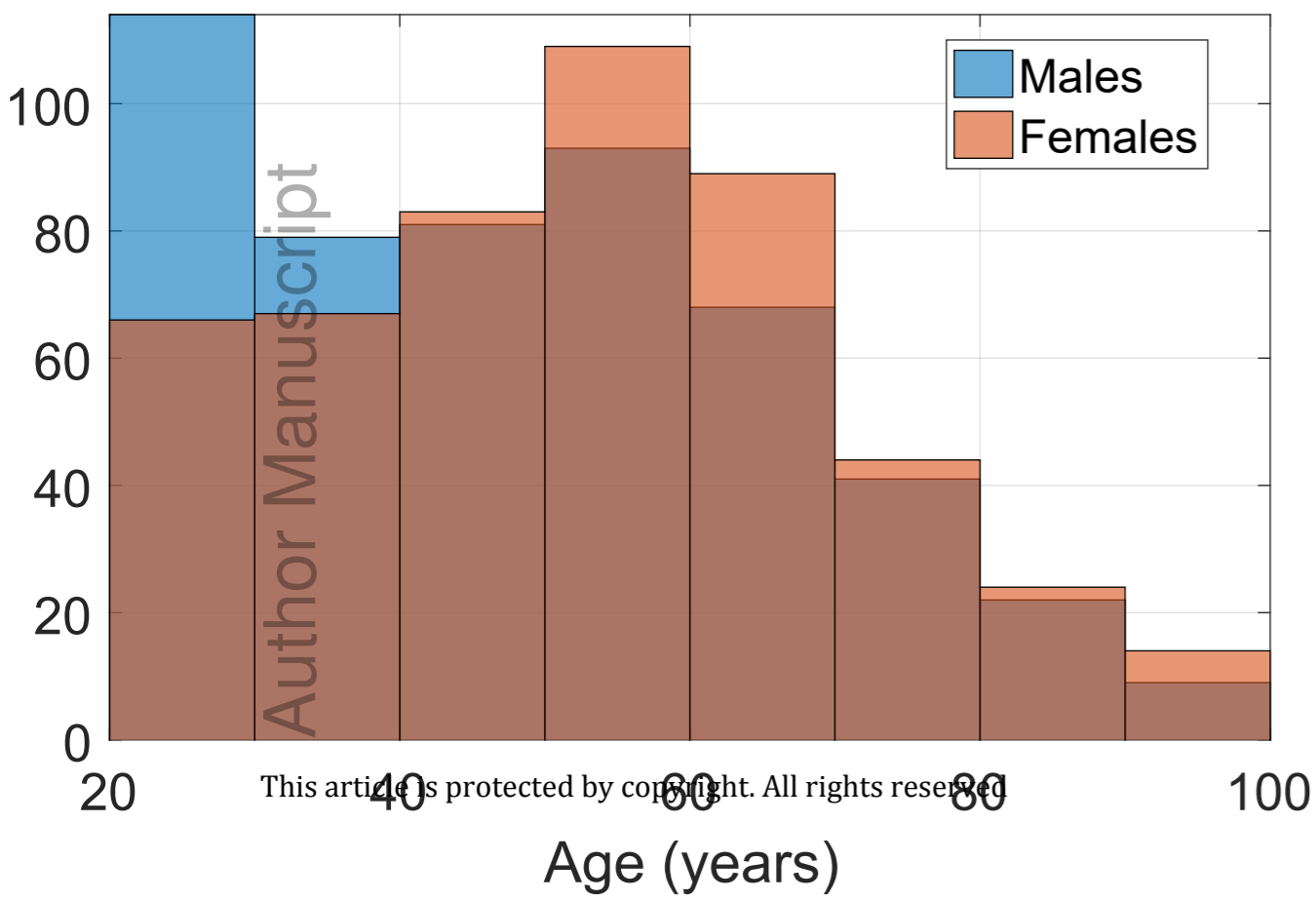
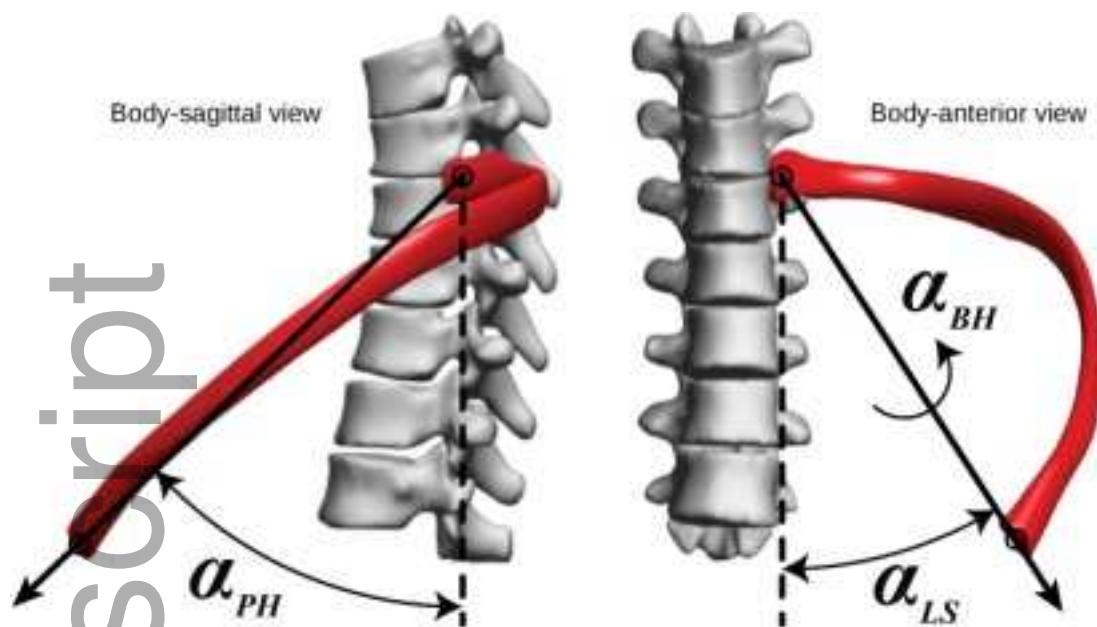


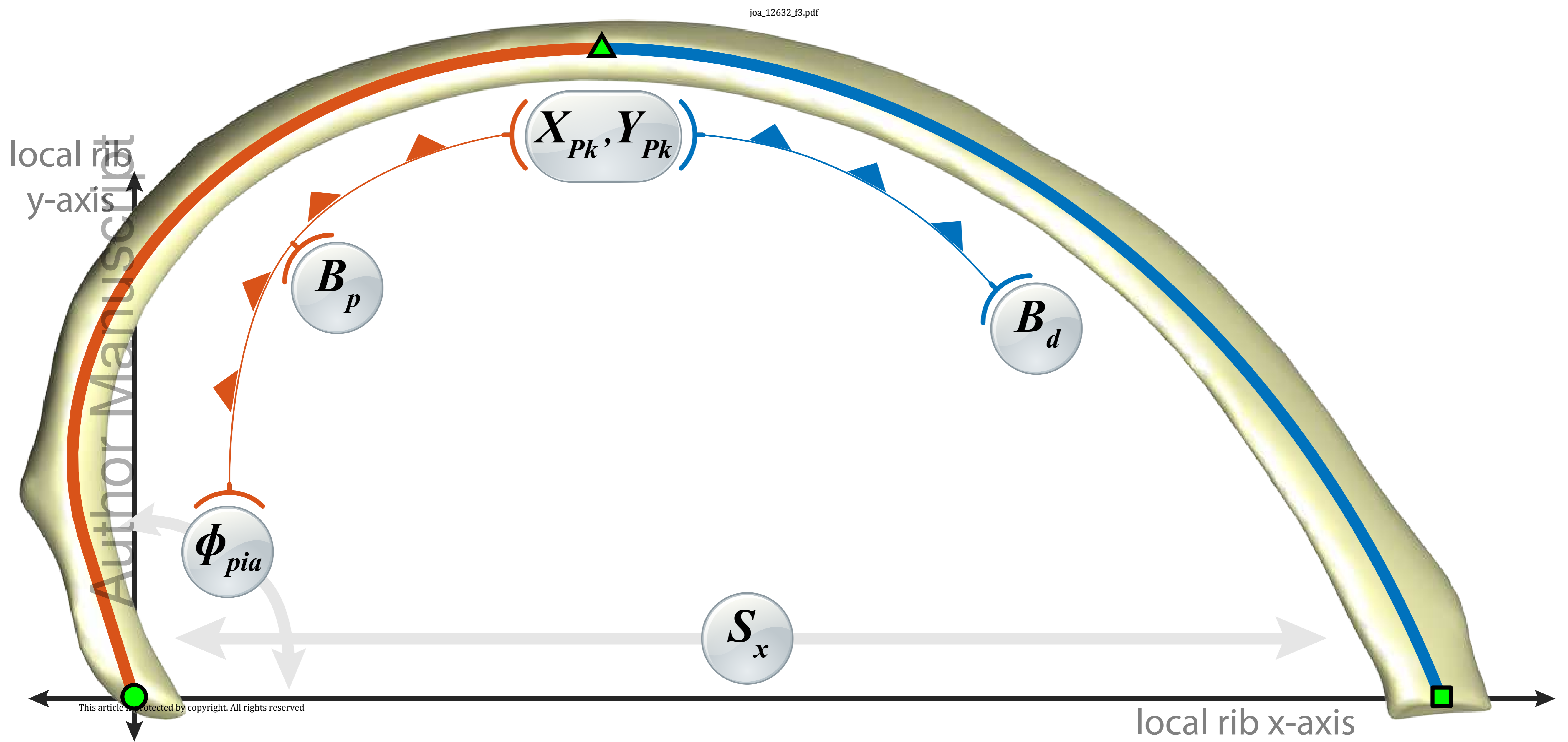
Figure A6: Expected values for rib arc length ( $L_{2d}$ ), inner angle at the distal end ( $\phi_{dia}$ ), and local curvature at posterior ( $\kappa_{post}$ ) and distal ( $\kappa_{dist}$ ) locations, along with values from rebuilt ribs matching that demographic. Regression models fitted to the values measured directly in the population are used to query for the expected values (with 95% confidence interval) for 95<sup>th</sup> percentile males of varying ages.





joa\_12632\_f2.png

Author Manuscript



local rib  
y-axis

$\Phi_{pia}$

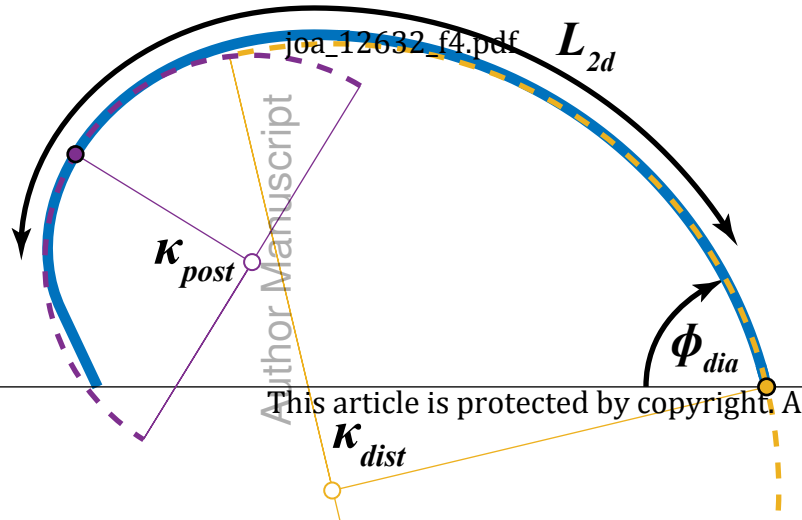
$B_p$

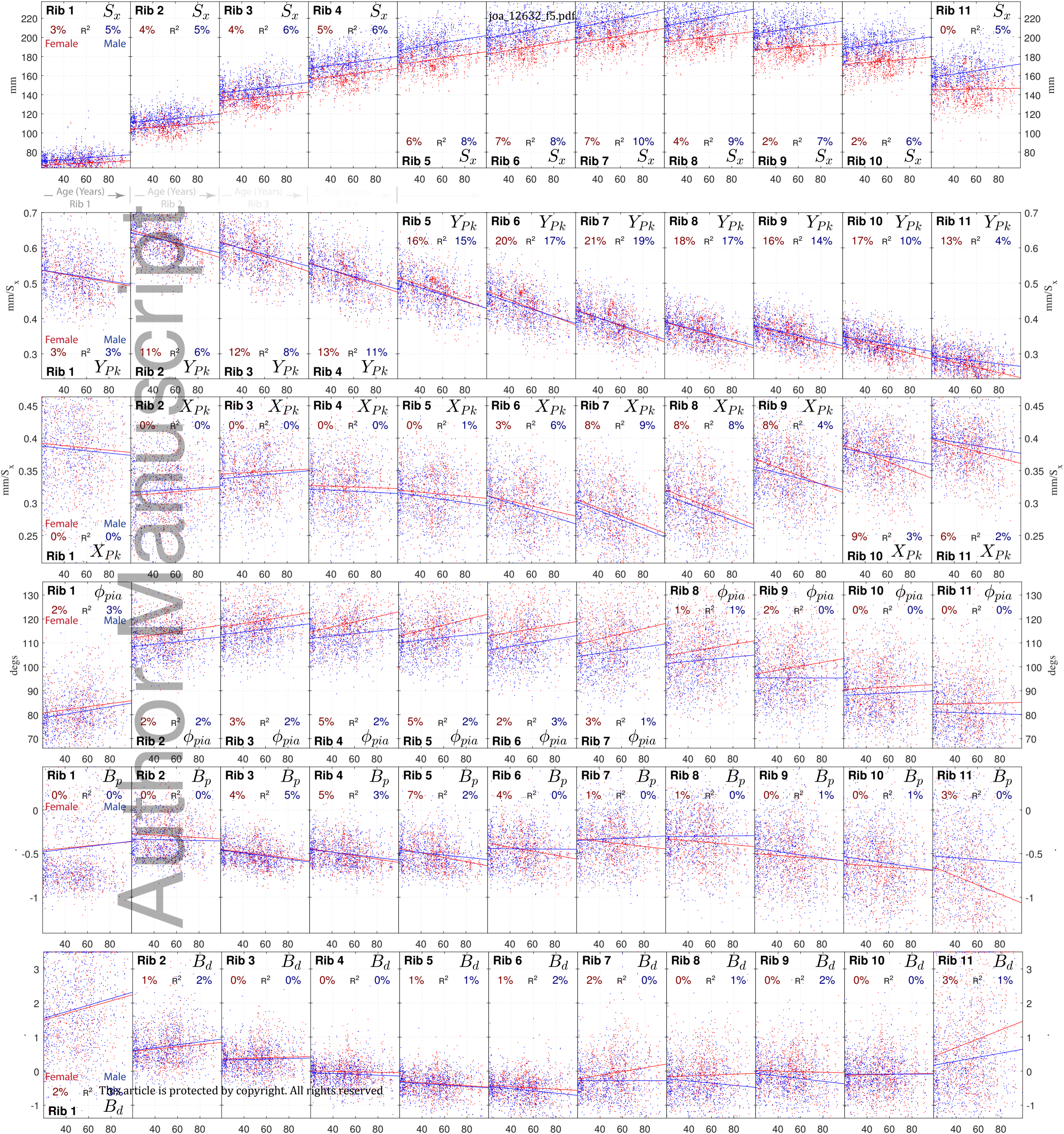
$(X_{Pk}, Y_{Pk})$

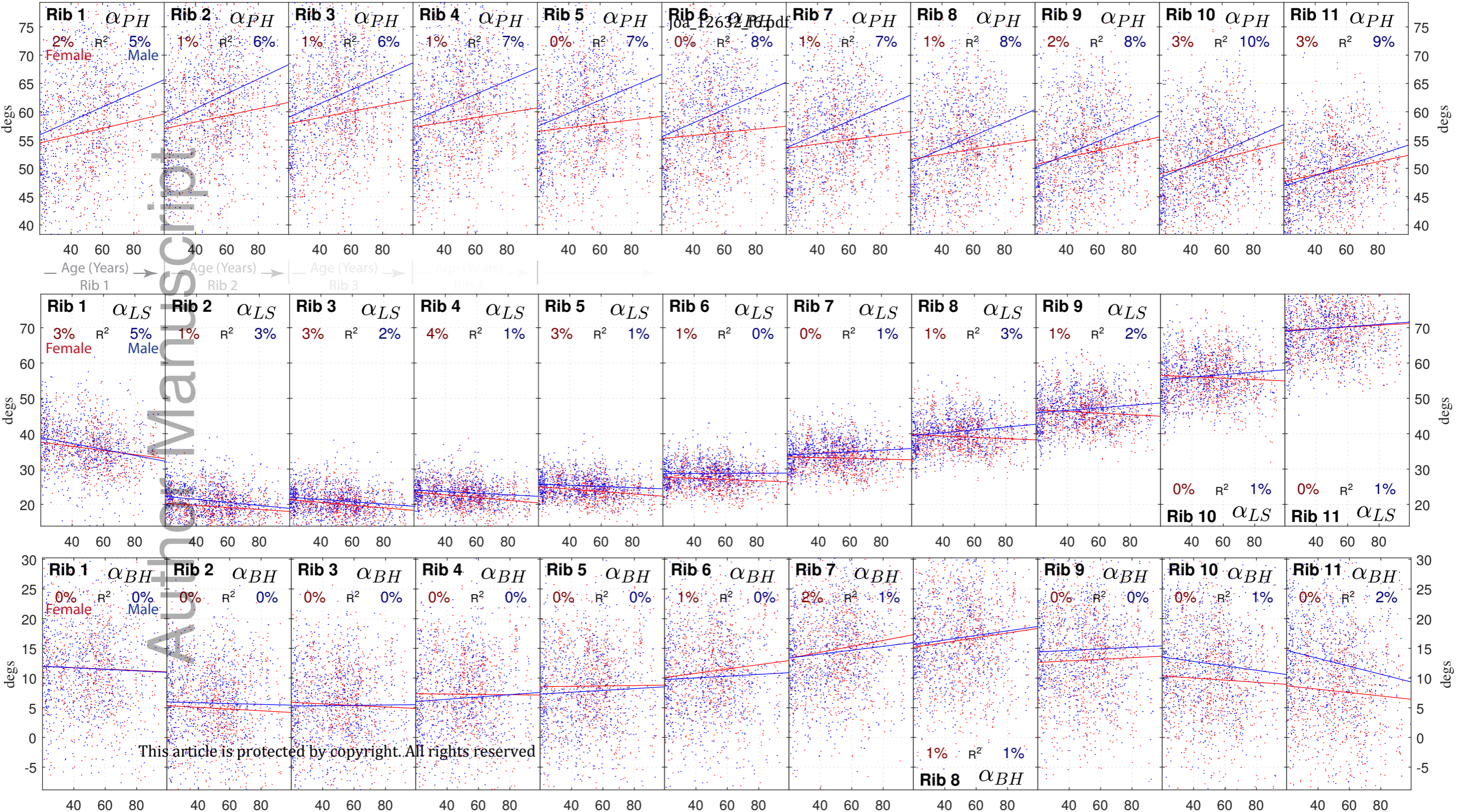
$B_d$

$S_x$

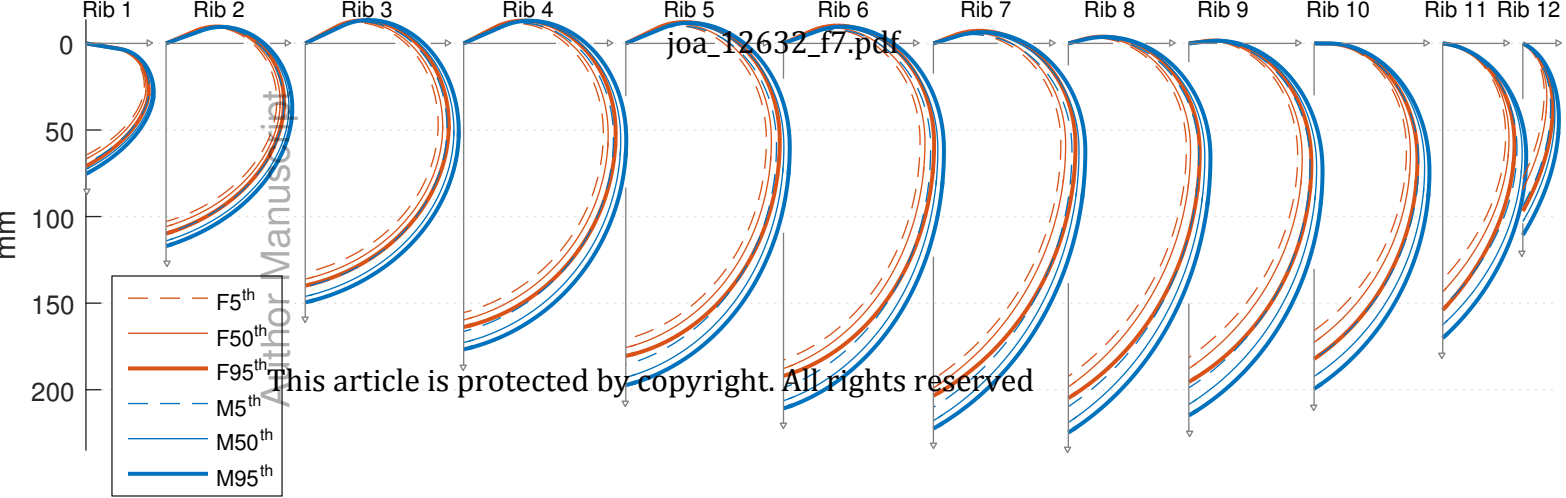
local rib x-axis

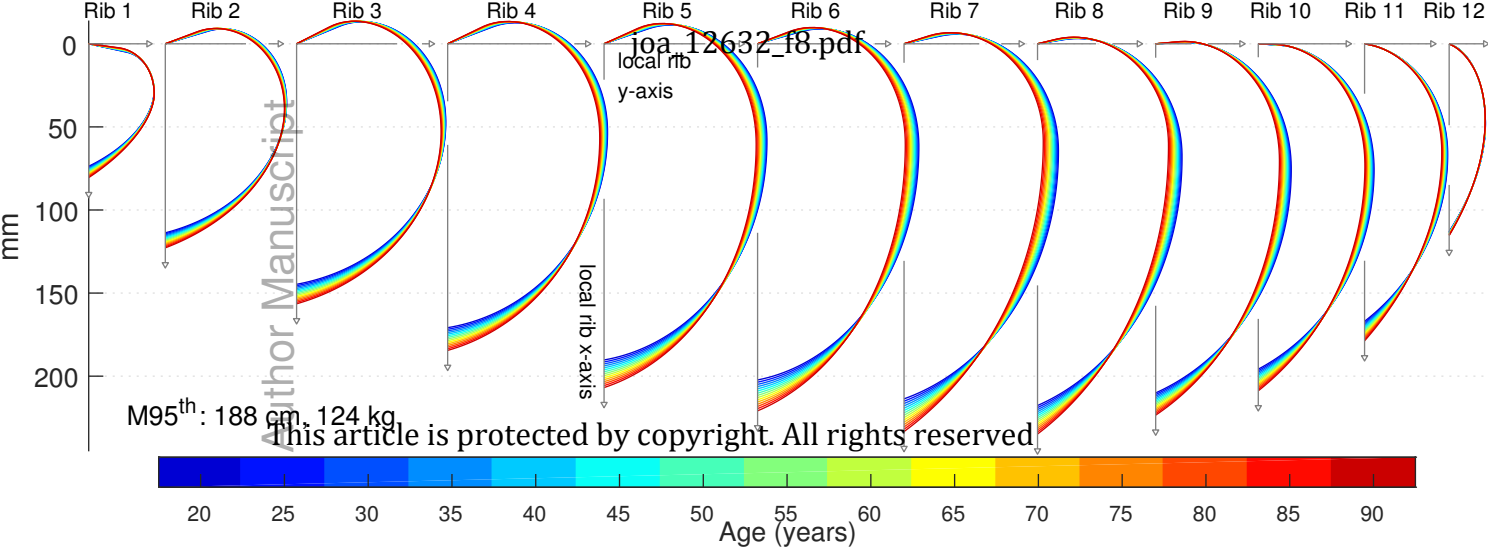


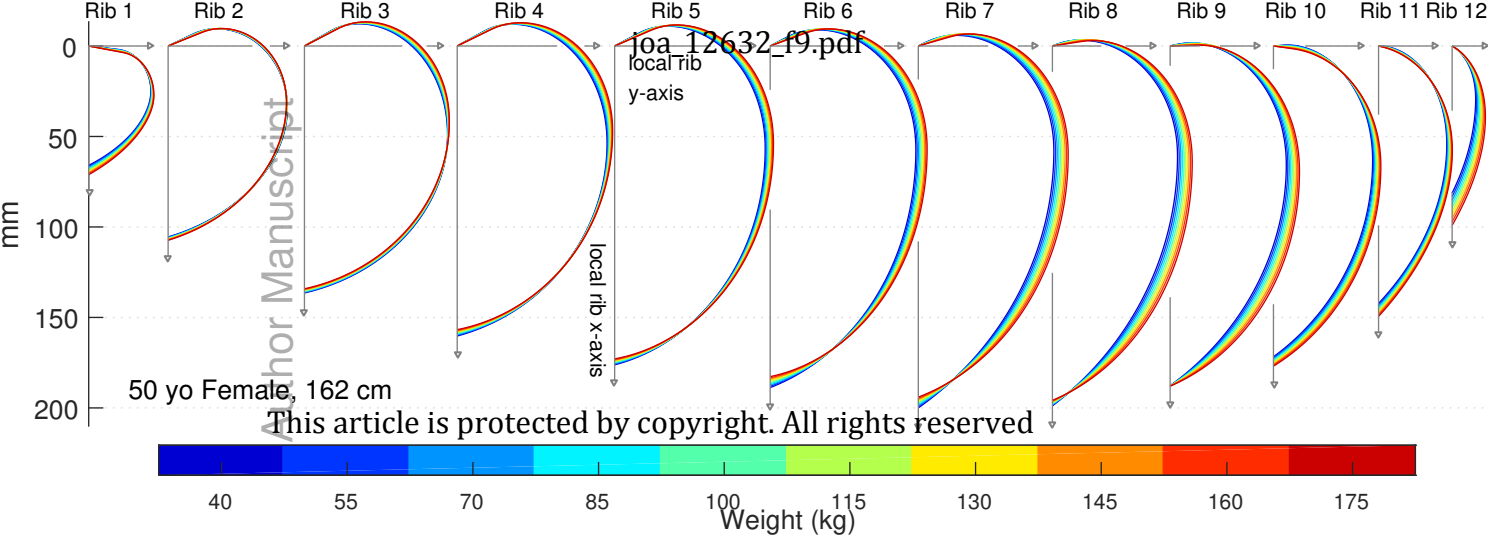


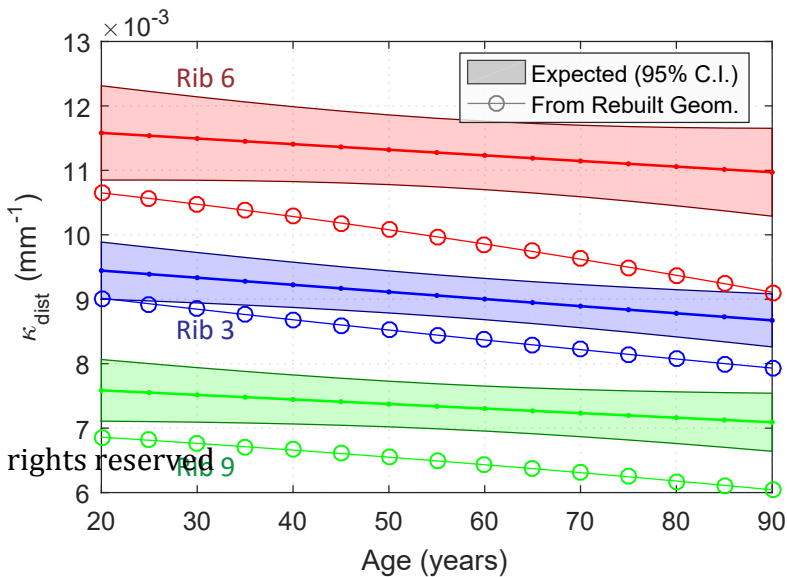
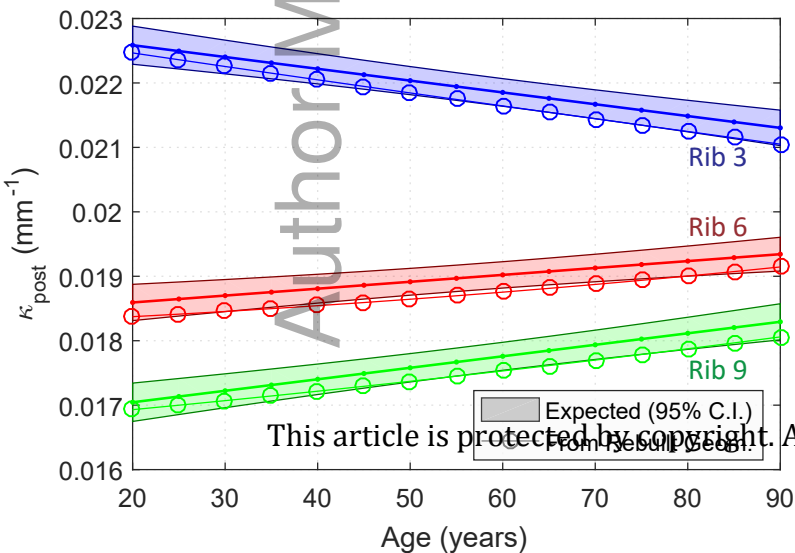
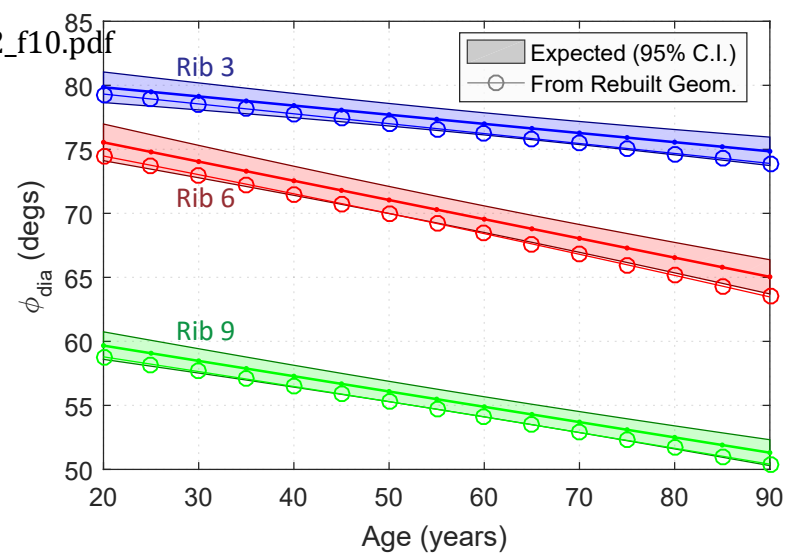
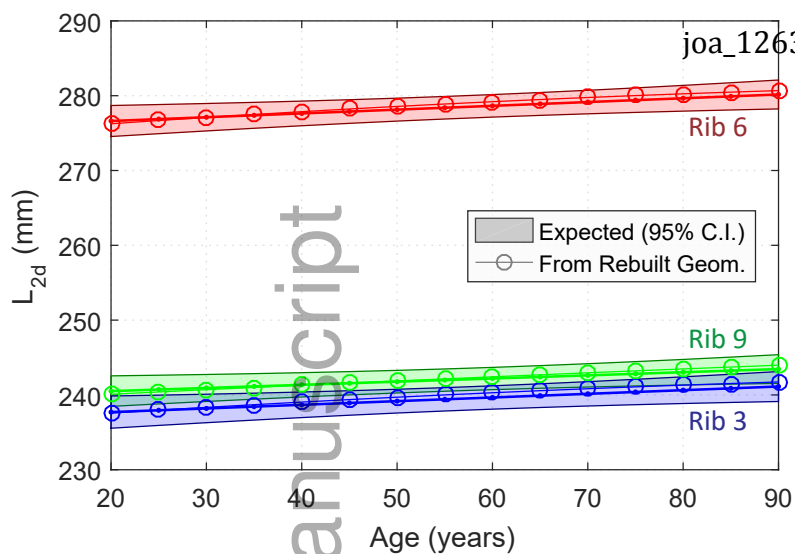












This article is protected by copyright. All rights reserved.